

Materials Horizons

Accepted Manuscript

This article can be cited before page numbers have been issued, to do this please use: J. A. Guerrero Teran, C. Plesse, V. Y. Shevtsov, A. S. Shaplov, J. Raquez and J. Odent, *Mater. Horiz.*, 2025, DOI: 10.1039/D5MH01784J.



This is an Accepted Manuscript, which has been through the Royal Society of Chemistry peer review process and has been accepted for publication.

Accepted Manuscripts are published online shortly after acceptance, before technical editing, formatting and proof reading. Using this free service, authors can make their results available to the community, in citable form, before we publish the edited article. We will replace this Accepted Manuscript with the edited and formatted Advance Article as soon as it is available.

You can find more information about Accepted Manuscripts in the [Information for Authors](#).

Please note that technical editing may introduce minor changes to the text and/or graphics, which may alter content. The journal's standard [Terms & Conditions](#) and the [Ethical guidelines](#) still apply. In no event shall the Royal Society of Chemistry be held responsible for any errors or omissions in this Accepted Manuscript or any consequences arising from the use of any information it contains.

Wider Impact statement

[View Article Online](#)
DOI: 10.1039/D5MH01784J

Piezoionic materials operate through mechanical-to-ionic transduction, generating transient voltages as ions of different mobilities separate under mechanical stimulation. Although the piezoionic effect is relatively new and its working principle is not yet fully understood, this review provides both material structural design guidelines for enhancing device performance and fundamental insights into the underlying transduction mechanisms. In addition, it outlines conceptual frameworks for translating the piezoionic effect into practical devices, emphasizing the role of operating parameters in voltage generation and strategies for engineering fluid-driven ion transport to further boost piezoionic responses.



Data availability

[View Article Online](#)
DOI: 10.1039/D5MH01784J

The review entitled “Boosting mechanical-to-ionic transduction for self-powered piezoionic sensing” by Juan A. Guerrero, Cédric Plesse, Vladislav Shevtsov, Alexander Shaplov, Jean-Marie Raquez, and Jérémy Odent does not contain any new data. Only previously published work has been cited.



REVIEW

Boosting mechanical-to-ionic transduction for self-powered piezoionic sensing

Juan A. Guerrero^a, Cédric Plesse^b, Vladislav Y. Shevtsov^{c,d}, Alexander S. Shaplov^c, Jean-Marie Raquez^a, and Jérémy Odent^{a*}Received 00th January 20xx,
Accepted 00th January 20xx

DOI: 10.1039/x0xx00000x

In the realm of sensing world, piezoionic systems have emerged as innovative tools for perceiving tactile sensations through mechanical-to-ionic transduction, mimicking biological signal production and transmission. Up to now, the biomimetic transduction mechanism and strategies to engineer the transduction efficiency remain not fully understood and underutilized. This review provides the fundamentals of mechanical-to-ionic transduction for efficient self-powered sensing, identifying the most crucial structural and operating parameters governing the generation of a transient signal output with respect to the migration and redistributions of ions upon mechanical stimulation. It also examines the recent strategies for efficiently converting mechanical keystrokes into electrical signals through performance-driven structural design, thereby maximizing piezoionic voltage generation. This involves engineering ion transport and fluid flow through porosity, microphase separation, conductive pathways and structural gradients. With respect to piezoionic effect-based applications, the review highlights the promising potential of polymeric ionic materials in soft wearable electronics, ionic skins, tissue engineering, biointerfaces and energy-harvesting.

From cellular mechanotransduction to biomimetic electromechanical transducers

Mechanotransduction is the process by which cells sense mechanical force and convert it into a biochemical response¹. As a cornerstone of the somatosensory system, this process supports critical physiological functions, at various levels, from whole-body systems to cellular and molecular processes including hearing, touch perception, and muscle contraction^{1,2}. Maksimovic *et al.*³ identified key proteins in skin mechanoreceptors that display touch-activated ionic currents, facilitating high spatio-temporal acuity for tactile perception. Under mechanical stimulation, the mechanosensitive ion-channel-based receptors transition between open and closed states. This creates an ion influx and generates an action potential which is relayed to the brain by the somatosensory system (Fig. 1)³⁻⁵. Each low-threshold mechanoreceptors are adapted to detect a particular stimulus and have a working range of frequency⁶⁻⁸. Merkel cell receptors optimally detect pressures below 2 Hz, Meissner corpuscles respond best to skin

movement and dynamic motion at 2-40 Hz, and Pacinian corpuscles are tuned to vibrations within a 40-200 Hz range⁸. Inspired by these natural mechanisms, soft electromechanical transducers have been designed to detect small changes in force, displacement, or vibration, converting the resulting mechanical stimuli into electrical signals⁹. While being increasingly valued for applications ranging from soft robotics to health monitoring, their most common transduction mechanisms include, until recently, piezoresistive, piezocapacitive, and piezoelectric mechanisms (Table 1)¹⁰⁻¹³. Despite their sensitivity to temperature, high hysteresis, poor linearity and long relaxation times, piezoresistive transducers enable to detect a wide range of detection-measuring pressures (ca. 1 Pa – 1 MPa), upon a change in resistance as a result of local mechanical deformations¹⁴⁻¹⁹. In the case of piezocapacitive transducers, they are still prone to hysteresis and to interferences (such as parasitic charges or electromagnetic noise) and offer a relatively high sensitivity to small pressures (ca. 1 Pa – 1 MPa), good temperature independence, and low power consumption. This is relied on the formation of an electrical double layer (EDL) at the dielectric-electrode interface, detect changes in capacitance through alterations in plate distance or electrical permittivity²⁰⁻²⁷. Standing out for high sensitivity, fast response time, mechanical flexibility, and chemical stability, piezoelectric transducers employ the ferroelectric properties of some (semi)crystalline and glassy materials to generate electric charges caused by stress-induced dipole rearrangement under dynamic or transient loads²⁸⁻³⁵. However, to achieve optimal piezoelectric performances, these materials require a poling step to align the dipole within the materials, and the range of pressure detected is generally higher (ca. 100 Pa – 10 MPa).

^a Laboratory of Polymeric and Composite Materials (LPCM), Center of Innovation and Research in Materials and Polymers (CIRMAP), University of Mons (UMONS), Place du Parc 20, Mons, 7000. E-mail: jeremy.odent@umons.ac.be

^b CY Cergy Paris Université, Laboratoire de physicochimie des polymères et des interfaces (LPPI) – LPPI, 5 mail Gay Lussac, Cergy-Pontoise Cedex F-95000, France

^c Functional Polymeric and Particulate Materials Unit, Luxembourg Institute of Science and Technology (LIST), 5 avenue des Hauts-Fourneaux, L-4362 Esch-sur-Alzette, Luxembourg

^d Department of Physics and Materials Science, University of Luxembourg, 2 Avenue de l'Université, L-4365 Esch-sur-Alzette, Luxembourg

* Electronic supplementary information (ESI) available. See DOI: 10.1039/x0xx00000x



REVIEW

Materials Horizons

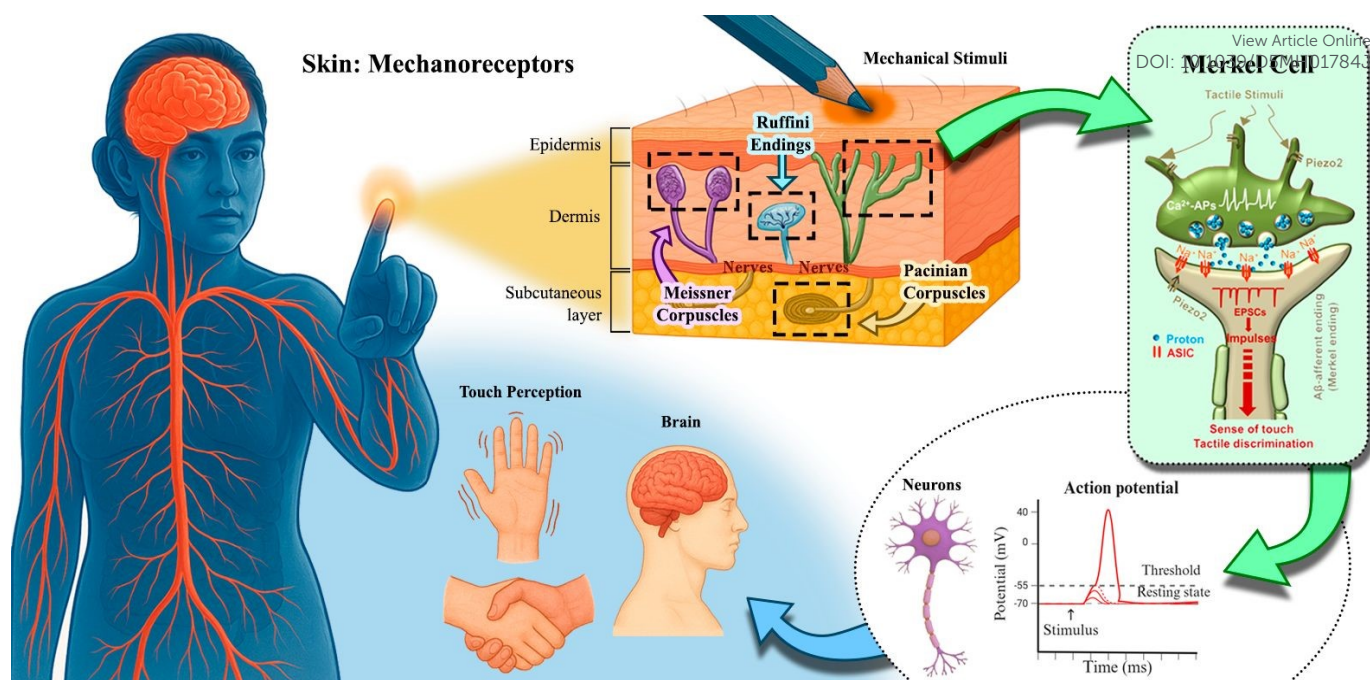


Fig. 1. Mechanisms underlying tactile perception and the different low-threshold mechanoreceptors on skin. Human skin mechanoreceptors transduce tactile stimuli into action potentials, which are transmitted via the afferent nervous system to synaptic junctions. At the synapses, action potentials relayed the information to the brain, giving rise to a complex multilevel feature of tactile perception. Reproduced under terms of the CC-BY license with permission⁶; Copyright Elsevier © 2024.

Inspired from biological systems, ionotronic devices, which couple electrons and ions movement, have led to the development of mechanical-to-ionic transducers such as piezoionics. These transducers operate via the flow of ions in a fluid or solid electrolyte^{9-10,36}. The piezoionic effect is relied on the newly discovered electromechanical conversion phenomenon that occurs when a non-uniform mechanical deformation is applied to ion embedded materials. This generates a transient voltage based on the separation of ions (cations and anions of different mobilities in the fluid transport)³⁷⁻³⁹. Often mistaken for piezocapacitive transducers due to the similarity of materials employed, piezoionic transducers afford a highly sensitive mechanical detection (*ca.* 1 Pa – 100 kPa) with a reliable linear response when converting mechanical loads into a proportional self-powered voltage output³⁷⁻⁴⁶. A fundamental distinction lies in power dependence as piezoresistive and piezocapacitive transducers require an external power supply to operate, whereas piezoelectric and piezoionic transducers are self-powered and generate an electrical signal autonomously. Besides, piezoelectric transducers are rather rigid, crystalline materials to generate voltage (*ca.* 0.01 V – 10 V) through atomic dipole displacement. In contrast, piezoionic transducers are relied on mechanically induced ion migration within soft, deformable, ionically conductive materials to generate transient voltage (*ca.* 1 – 500 mV)³⁷⁻⁴⁶. Up to now, piezoionic transducers exhibit a response time in the range of milliseconds to seconds but a slow recovery time in the range of tenths of a second to tens of seconds when compared to other types of electromechanical transducers. Overall, the electromechanical performance of soft electromechanical transducers is dictated by major parameters such as sensitivity, detection limit, operating pressure range,

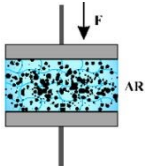
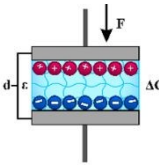
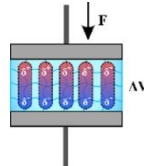
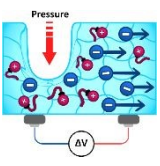
response time, self-powering and linearity. These attributes enable soft electromechanical transducers to be easily integrated and to continuously monitor and detect a wide range of mechanical loads with high resolution¹⁰⁻¹³. To that end, **Table 1** provides a conceptual comparison of the different electromechanical transducers with respect to a survey of the current state of the art in terms of their sensitivity and maximum pressure limit as shown in **Fig. 2**. From an application standpoint, the detection pressure range of piezoionic transducers makes them promising candidates for wearable sensors and electronic skin technologies. Their high sensitivity to subtle forces, combined with self-powered voltage output and good linearity, allows them to detect mechanical stimuli ranging from ultra-light touch to soft deformations, *i.e.* well within the sensitivity range of human skin, which typically begins to perceive pressure around 10 – 100 Pa.

There are several reviews that previously introduced the piezoionic effect, by stressing out the historical evolution, scientific description, methodology, application, and outlook⁴⁷⁻⁴⁸. While Ho *et al.*⁴⁷ provides a holistic overview of early conceptualization of piezoionics as a biomimetic mechanical-electrical transduction mechanism, Chen *et al.*⁴⁸ rather highlighted the different types of piezoionic materials and methods to enhance the piezoionic response. In contrast, the review serves as a guide for newcomers to the field as it provides insights into the fundamentals of the mechanical-to-ionic transduction, including an up-to-date description of recent polymeric ionic materials used, the crucial structural and operating parameters governing the voltage generation. Moreover, the recent innovative strategies to engineer ion transport and fluid flow for maximizing piezoionic performance



and a brief exploration of relevant applications are addressed in the review.

Table 1. Conceptual distinction between piezoresistive, piezocapacitive, piezoelectric and piezoionic electromechanical transducers.

Piezoresistive	Piezocapacitive	Piezoelectric	Piezoionic
			

Open Access Article. Published on 05 december 2025. Downloaded on 7.12.2025 12:07:04.
This article is licensed under a Creative Commons Attribution-NonCommercial 3.0 Unported Licence.



Transduction mechanism	Change in the percolation or conductive pathways	Alterations in plate distance or electrical permittivity	Change in polarization	Ion redistribution
Signal output	Change in resistance (ΔR) Current change (ΔI)	Change in capacitance (ΔC)	Voltage generation (V) Current change (ΔI)	Ionic potential change (ΔV) Current change (ΔI)
Signal output range	10 – 10,000 Ω	0.001 – 1 nF	0.01 – 10 V	1 – 500 mV
Detection pressure range	1 Pa – 1 MPa	1 Pa – 1 MPa	100 Pa – 10 MPa	1 Pa – 100 kPa
Sensitivity	1 – 1000 kPa ⁻¹	1 – 100 kPa ⁻¹	0.1 – 100 kPa ⁻¹	0.001 – 100 kPa ⁻¹
Response time	ms – s	ms – s	ms – s	ms – s
Recovery time	ms	ms	ms	0.1 s – 10 s
Advantages	Good stability	Good temperature independence Low power consumption	Self-powered Mechanical and chemical stability High output voltage	Self-powered Good linearity Mechanically soft and deformable
Disadvantages	Temperature sensitive High hysteresis Poor linearity Long relaxation time External power supply required	Prone to hysteresis and to interferences External power supply required	Only detect dynamic or transient loads Poling required Mechanically rigid	Moisture and temperature sensitive Low output voltage

Conceptual frameworks for mechanical-to-ionic transduction

Initially identified by De Gennes *et al.*⁴⁹ within ionic gels, the concept of mechanical-to-ionic transduction was coined as the piezoionic effect by Sarwar *et al.*³⁷. The piezoionic effect is the transient separation between anionic and cationic species in response to an applied mechanical stress (Fig. 3)^{38–39}. Under mechanical stimulation, a fluid pressure gradient is created, which drives fluid flow within the matrix. As a result, cations and anions are carried by the fluid flow but at different speeds due to their different mobilities and interaction with the polymer matrix. This in turn generates a transient voltage according to the leading/dominant ion (the most mobile)^{38–39}. Overall, the generated potential generally exhibits a linear relationship with the pressure gradient, as shown in eq. 1 where α is the charge accumulation and electrical potential generation^{44,49}. Although being effective for piezoionic systems built on a single mobile ion, this model is inaccurate for ion-pair (involving two mobile ions) since it only considers the ions transport within the fluid flow due to pressure gradient generation. As a result, the model suggests that the larger the fluid flow speed, the higher the piezoionic response^{44,49}.

The Poisson-Nernst-Planck (PNP) equations are another foundation for studying ion transport in fluids, describing ionic transport under the influence of gradients and electric fields^{38,39,50–51}. Therein, the Nernst-Planck equation considers ion transport based on the mass transport phenomena of diffusion, electromigration, and convection whereas the Poisson equation explains the distance

charge distribution of ions, owing to an electric field, respectively defined in eq. 3 and eq. 4 where J_i is the ion flux, D_i is the diffusion coefficient of ion i , c_i is the concentration of such ion, z_i is the electron valence of the ion, k_B is Boltzman constant, T is temperature, e is the fundamental charge, v is the flow velocity, V is the electrical potential, and ϵ is the permittivity of the medium^{38,39,50–51}:

$$J_i = -D_i \nabla c_i - D_i \frac{e}{k_B T} z_i c_i \nabla V + v c_i \quad (\text{eq. 3})$$

$$\nabla^2 V = \frac{\sum z_i e c_i}{\epsilon} \quad (\text{eq. 4})$$

This model can effectively capture ion movement in biological systems, such as cells and channels^{50–51}. Nevertheless, PNP model has limitations, such as neglecting ion-ion interactions, steric hindrance, and finite volume effects^{52–53}. As such, a modified PNP model considering such effects led to eq. 5 where the term a^3 is the spacing between densely packed ions, which correlates to the concentration limit $a^3 = 1/c_{\max}$ ^{52–53}:

$$J_i = -D_i \nabla c_i - D_i \frac{e}{k_B T} z_i c_i \nabla V - a^3 D_i \nabla \cdot \left(\frac{c_i \nabla (c_+ + c_-)}{1 - a^3 c_+ - a^3 c_-} \right) + v c_i \quad (\text{eq. 5})$$

As the mechanical-to-ionic transduction critically depends on the fluid flow to generate a transient voltage with respect to the transient separation of cations and anions at different speeds, it can be mechanistically analyzed by Darcy's law. The latter describes the velocity of a fluid traveling through a porous medium with respect to



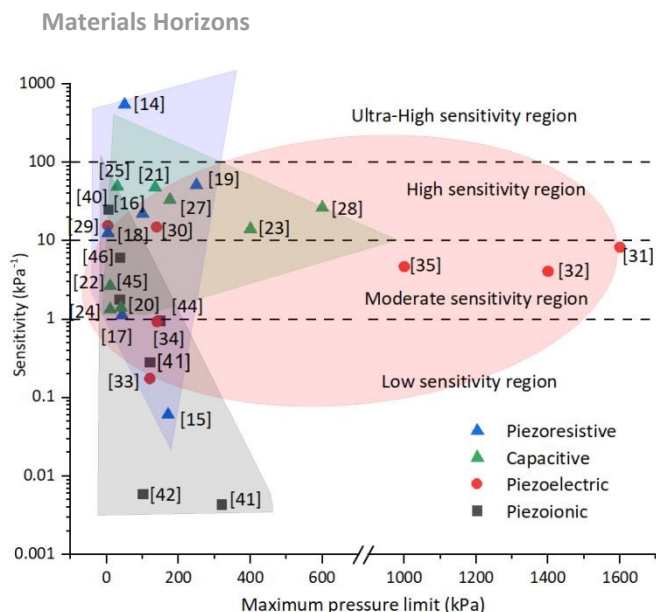


Fig. 2. Sensitivity (kPa^{-1}) and maximum pressure limit (kPa) of common piezoresistive, capacitive, piezoelectric and piezoionic electromechanical sensors.

eq. 6 where v is the flow velocity, κ is the permeability, η is the viscosity, and ΔP is the pressure gradient ³⁸:

$$v = -\frac{\kappa}{\eta} \Delta P \quad (\text{eq. 6})$$

Dobashi *et al.* ³⁸ combined the PNP equations (**eq. 3** and **eq. 4**) with Darcy's law (eq. 6) to better understand the mechanical-to-ionic transduction in dilute media where ion-ion interactions are negligible as well as for ion-pair systems (involving two mobile ions). This leads to **eq. 7** where N is the number of ions, e is the fundamental charge, κ is the permeability, η is the viscosity, σ is the conductivity, D_{o+} and D_{o-} are the diffusion coefficients of the cation and anion without drag forces and interactions with the matrix, respectively, while D_+ and D_- are the effective diffusion coefficients of the cation and anion, respectively ³⁸:

$$\Delta V = -\frac{eN\kappa}{\sigma\eta} \left[\frac{D_+}{D_{o+}} - \frac{D_-}{D_{o-}} \right] \Delta P \quad (\text{eq. 7})$$

In the present model, mechanical stress creates a fluid flow (convective flux) that drives ionic movement and induces charge separation due to differences in ion mobility ³⁸. Unlike the streaming model (eq. 2), the latter approach considers not only fluid-driven ion transport but also the different mobilities of individual ions. As a result, the dominant ion (the most mobile) drives the voltage generation with respect to the diffusion coefficients, which in turn depend on ion size, matrix porosity, permeability, and ion-matrix interactions. Therein, larger fluid flow speed and larger mobility difference between the ions produce higher output voltage ³⁸. Wang *et al.* ⁵² proposed a different model based, this time, on the modified PNP (eq. 5), coupled with Darcy's law (eq. 6), yielding to **eq. 8**:

$$\nabla V = \frac{c_i \frac{-\kappa}{\eta} \Delta P - a^3 D_i \nabla \cdot \left(\frac{c_i \nabla (c_+ + c_-)}{1 - a^3 c_+ - a^3 c_-} \right)}{\frac{e_0}{K_b T} z c_i} \quad (\text{eq. 8})$$

While the previous model considered the spacing of ions and ion-ion interactions, the later have (**eq. 7** and **eq. 8**) been successfully applied on ion-pair systems, appropriately predicting the voltage generation ⁵².

Sensor composition and structural design factors affecting piezoionic performance

DOI: 10.1039/D5MH01784J

Piezoionic transducers operate by mechanically stimulating a polymer matrix or a gel, which generates a fluid pressure gradient that, in turn, drives ion flow within the matrix. As a result, a transient separation between cations and anions takes place due to their different mobilities and interaction, breaking electrical neutrality and generating a transient voltage ³⁸⁻³⁹. Thus, the polymer matrix and the ions are among the key factors influencing the performance of the piezoionic sensor. Structural parameters such as the type of polymer matrix, its dimensions, the nature and mobility of the ions, the presence of liquid ion transporters, the charge density, the crosslinking density, porosity, microphase separation, and introduction of a predetermined gradient of ions, significantly affect fluid-driven ion transport (**Fig. 3**). In the following sections, we will examine and analyse each of these structural parameters in detail. Unfortunately, unlike to the well-established measurement of ionic conductivity or cycling of batteries, there is no common practice for the assembly and testing of piezoionic sensors. This makes the comparison of the results and performance analysis of reported sensors quite a challenging task. Thus, we propose evaluating their performance based on the generated voltage range and the levels of applied pressure or strain forces. The key considerations include the maximum generated voltage, which facilitates future sensor applications, and the minimum applied force, which determines the device's sensitivity. These performance parameters are summarized in **Table 2**. Another important parameter for evaluating sensor performance is the response speed, or relaxation time, that is, the time required for the sensor to return to its initial state and become ready to generate a new response. However, the majority of reported studies have concentrated on the dependence of generated voltage on the applied mechanical force, whereas only a limited number have examined repeated cycling, which is necessary to assess the relaxation time. Consequently, this parameter was not considered in the current review. As a result, piezoionic sensors can be categorized as follow:

1. Type of polymer matrix and ionic species

The known piezoionic sensors can be categorized into the five groups based on the type of polymer matrix used:

I. Neutral polymers with ionic liquids (Table 2, entries 1–8).

The first group consists of commercially available neutral polymers doped with ionic liquids (ILs). Poly(vinylidene fluoride-hexafluoropropylene) (PVDF-HFP) ^{46,54} and thermoplastic polyurethanes (TPU) ⁵⁵⁻⁵⁹ are the most commonly used matrices

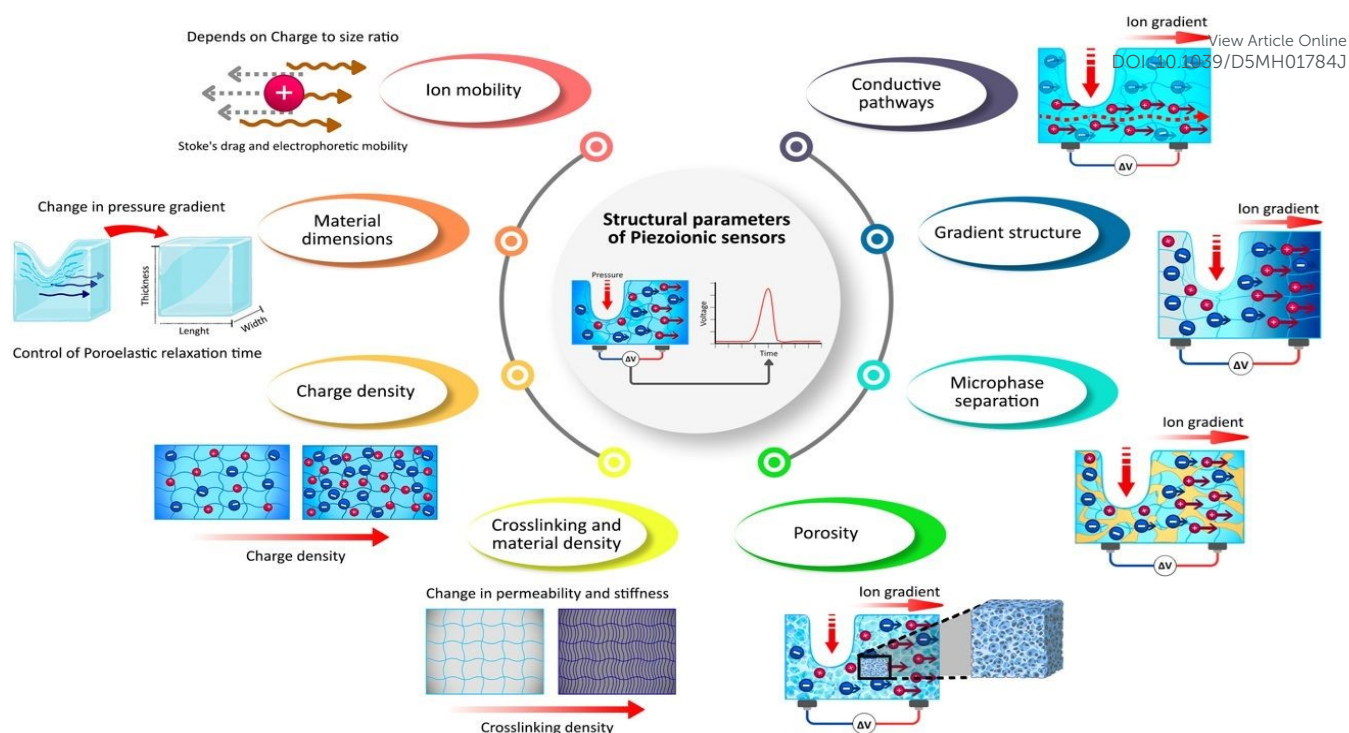


Fig. 3. Structural parameters affecting the fluid-driven ion transport including ion mobility, material dimensions, charge density, crosslinking density and material density (left, red to yellow from material selection) and porosity, microphase separation, gradient structure and conductive pathways (right, green to purple from structural design).

due to their ability to form tough, elastic films, even at high filler loadings that exceed the polymer mass. These sensors contain both mobile cations and anions, contributing to ion migration under mechanical stress. It is worth noting that 1-ethyl-3-methylimidazolium bis(trifluoromethylsulfonyl)imide ($\text{EMIm}^+ \text{TFSI}^-$) and 1-ethyl-3-methylimidazolium tetrafluoroborate ($\text{EMIm}^+ \text{BF}_4^-$) are among the most commonly used ILs due to their high ionic conductivity, as well as exceptional thermal and electrochemical stability.

II. Neutral hydrogels with metal salts (Table 2, entries 9–14).

The most commonly used hydrogels are based on water-soluble polyacrylamide (PAAm) matrices crosslinked with bisacrylamide or with various poly(ethylene glycol) diacrylates (PEGDA)^{40, 42, 45, 52, 60–61}. To improve their mechanical stability in the swollen state, some linear polymers such as poly(vinyl alcohol) (PVA) or PVDF-HFP were incorporated into the crosslinked PAAm network, forming semi-interpenetrating structures^{52, 55}. Following the synthesis, these crosslinked polymers were impregnated with aqueous solutions of different metal salts, including NaCl, LiCl, KCl, $\text{KFe}[\text{CN}]_6$ or CaCl_2 ^{42, 45, 52, 60–61}.

III. Polyelectrolyte ion gels with ionic liquids (Table 2, entries 15–16).

The third group comprises polyelectrolyte-based sensors filled with ILs, with Nafion and its analogs being the most frequently used materials^{56, 62}. Since anions are chemically bonded to the polyelectrolyte backbone, a stable ion concentration gradient is formed within the polymer matrix under applied force, that is supposed to further enhance the piezoionic response.

IV. Polyelectrolyte hydrogels (Table 2, entries 17–22).

This class of polymer matrices is typically synthesized by crosslinking ionic monomers, either cationic or anionic, with multifunctional neutral crosslinkers in aqueous solution^{38, 41, 43–44}. Commonly employed ionic monomers include [2-(acryloyloxy)ethyl]trimethylammonium chloride, 3-sulfopropyl acrylate potassium salt^{43–44}, and acrylic acid^{38, 41}, which provide mobile counterions such as chloride (Cl^-), potassium (K^+), or protons (H^+). To obtain hydrogels with controlled sizes and complex geometries, 3D printing techniques have been successfully applied, as demonstrated by Odent *et al.*^{43–44}. Notably, these polyelectrolyte hydrogels typically contain only a single type of mobile ionic species, which simplifies the generation of ion gradients under applied mechanical deformation.

V. Solid-state polyelectrolytes (Table 2, entries 23–28)

The final category comprises fully solid-state sensors constructed exclusively from charged polymers, either anionic^{63–66} or cationic^{66–67} polyelectrolytes. Among polymers bearing covalently bound anions, the commercially available Nafion has been frequently employed^{63–65}. In other studies, anionic or cationic ionic liquid like monomers (ILMs) were selected as precursors, as their polymerization yields poly(ionic liquid)s (PILs) with inherently high ion mobility, a key factor for efficient sensor response. A major challenge in PIL-based systems is balancing ionic conductivity (ion mobility) with mechanical robustness (viscoelastic properties). To address this, ILMs are often crosslinked to produce tough yet elastic films⁶⁶. An alternative approach, introduced by Ribeiro *et al.*⁶⁷, involves the design of semi-interpenetrating networks (semi-IPNs)



combining a linear conductive PIL with a reinforcing polyethylene oxide matrix, specifically a synergistic composition was achieved with better mechanical properties and ionic conductivity compared with its individual components.

2. Single-ion vs. ion-pair mobility

Among these five categories mentioned, we can classify into two large classes: systems where both cations and anions are mobile (I–III, ion-pair mobility) and systems with only a single mobile ion (IV–V, single-ion mobility), as illustrated in Fig. 4. In the systems containing two mobile ionic species (metal salts or ILs), the mechanical-to-ionic transduction is dictated by the transient charge separation caused by the strain-driven ion flux and the preferential displacement of the cations over anions, and vice versa. Enlarging the difference in mobility between anions and cations results into an amplified ionic gradient, thereby generating an enhanced voltage response. In this context, an enhanced voltage response is typically observed in systems where the polymer matrix is modified to either selectively facilitate or hinder ion migration. Such modifications (Table 2, entries 1, 2, 6) give rise to ion-selective transport, driven by specific ion-matrix interactions^{46, 54, 58}. For instance, Lee *et al.*⁵⁸ showed that incorporating EMIm⁺TFSI[−] ionic liquid into a TPU matrix resulted in a cation-driven piezoionic response (Table 2, entry 6). This behavior was attributed to stronger ion-dipole interactions between the TPU matrix and the TFSI[−] anion, rendering EMIm⁺ more mobile than TFSI[−]. Similarly, Weiyan *et al.*⁴⁶ utilized a PVDF-HFP matrix to enhance TFSI[−] mobility, as strong dipole interactions preferentially immobilized EMIm⁺ (Table 2, entry 1). When different EMIm-based ILs were incorporated into a TPU matrix (Table 2, entries 3–8), the generated voltage remained low, regardless of the electrode type. Sensors with EMIm⁺TFSI[−] produced voltages in the range of 0.5–4.5 mV^{55–56, 58}, whereas replacing TFSI[−] with BF₄[−] anion (EMIm⁺BF₄[−]) increased the response up to 11 mV⁵⁹. This enhancement can be attributed to the smaller size of BF₄[−], which increases the relative mobility difference between BF₄[−] and EMIm⁺ under the same strain. More generally, it can be speculated out that the limited performance of TPU-based systems may result from the hard segments of TPU chains, which restrict ion mobility and thus suppress voltage generation. In contrast, when EMIm⁺TFSI[−] was embedded in a PVDF-HFP matrix (Table 2, entries 1–2), the sensors displayed significantly superior piezoionic responses^{46, 54}. Remarkably, output voltages of 90–95 mV were reported, representing a substantial improvement over TPU-based systems. This enhanced performance can be attributed not only to the use of PVDF-HFP, but also to specific structural features embedded within these sensors. Even when EMIm⁺TFSI[−] was replaced with the less conductive LITFSI propylene carbonate solution (Table 2, entry 9)⁴⁰, and PVDF-HFP was used without additional structural modifications, the resulting sensor still outperformed TPU-based ones, generating voltages of up to 15 mV. However, switching from neutral polymers to charged Nafion filled with EMIm⁺TFSI[−] (Table 2, entries 15–16) did not lead to a significant improvement in output voltage, regardless of the electrode type^{56, 62}. This limitation is likely due to ionic interactions and ion-exchange processes involving the covalently bound SO₃[−] groups, H⁺ counterions, and the EMIm⁺TFSI[−] ion pairs. Such interactions likely

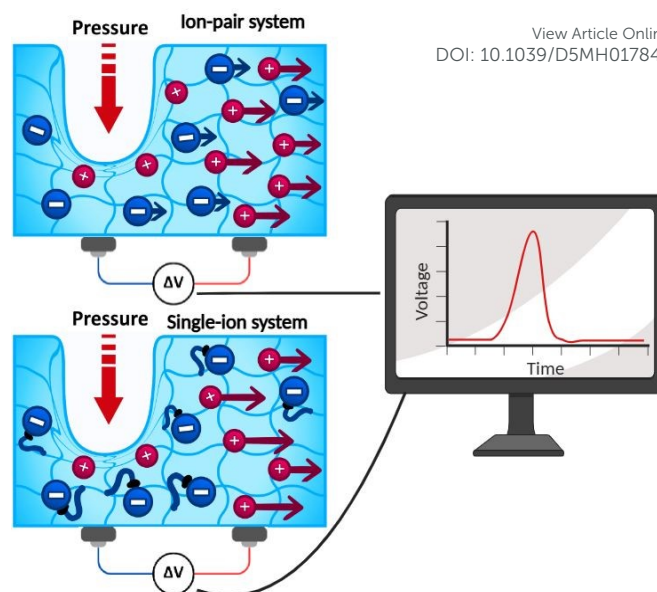


Fig. 4. Mechanical-to-ionic transduction of single-ion and ion-pair based ionic materials, leading to transient voltage generation with respect to the transient separation of anionic and cationic species in response to an applied mechanical load.

restrict ion mobility in response to mechanical stress, thereby diminishing the mechanical-to-ionic transduction.

Single-ion conducting matrices (Table 2, 17–28) are particularly attractive for piezoionic sensing, as they are expected to promote stronger and more stable ion-gradient formation under mechanical stress. Compared with ion-pair systems, single-ion systems offer distinct advantages, most notably the ability to differentiate between transient and static loads^{38, 44}. Under a transient mechanical stimulus, the applied stress induces a voltage that relaxes once the load is released, resulting in a transient recovery. By contrast, a static load leads to a gradual reduction of the fluid pressure gradient, slowing down fluid flow and causing voltage decay over time³⁸. In ion-pair systems, this effect is exacerbated because the imbalance between cation and anion distributions is inherently short-lived³⁹, leading to significant voltage loss. However, the charge separation persists over longer timescales, thereby reducing voltage decay and enabling more reliable sensing performance. Finally, the performance of single-ion conducting systems strongly depends on the mobility of the free ions. This mobility is influenced by multiple factors, including the type of anions and cations, the nature and length of the spacer between the polymer backbone and the covalently bound ion, the type of crosslinker, and the presence of specific interactions between the polymer matrix and the mobile ions. For a more detailed discussion of these factors, readers are referred to recent reviews on PILs^{68–69}. Considering all the advantages of gradient ion distribution under mechanical load in single-ion conducting matrices, it was anticipated that well-designed polymer matrices would enable sensors with excellent performance. Two notable examples are systems based on Nafion (Table 2, entry 25)⁶⁵ and conductive crosslinked PILs (Table 2, entries 26–27)⁶⁶, which delivered some of the highest output voltages among the cases summarized in Table 2. Even when polyelectrolytes were combined with relatively less mobile ions such as K⁺ and Cl[−]



(compared with H^+ , BMI^+ , or $TFSI^-$), their formulation as hydrogels allowed water to act as an ion transporter, enabling the generation of voltages as high as 70 mV under a 22.5 kPa load ⁴⁴.

3. Hydrogels/ionogels vs. solid-state systems

When it comes to hydrogels and organogels^{38-45, 52, 60-61}, both the magnitude and response speed of the generated voltage depend not only on the transport of mobile ions but also on the movement of solvent molecules solvated ion-pairs ⁷⁰. On one hand, the presence of water as an ion transporter greatly facilitates ion mobility, leading to unprecedented levels of ionic conductivity and, in turn, enabling ultrafast response and exceptionally high voltage output (Table 2, entries 11-13) ^{45, 52, 60}. Although direct comparison is complicated by differences in assembly and testing methodologies, both neutral polymers (Table 2, entries 11-13)^{45,52,60} and polyelectrolytes (Table 2 entries 21-22)⁴⁴, when swollen in water or aqueous salt solutions, were able to deliver high sensitivity and strong voltage responses. Since water readily evaporates, it has been partly substituted with the less volatile glycerol (Table 2, entries 21-22) ⁴⁴. This modification yields ionically conductive gels with enhanced stability under open-air conditions, while still achieving output voltages of up to 70 mV under a 22.5 kPa load. However, despite these impressive sensing performances, solvent evaporation remains a major limitation for the practical application of such systems in sensors. Unlike hydrogels or organogels, ionogels (Table 2, entries 15-16) are inherently non-volatile, as ionic liquids possess nearly zero vapor pressure ^{56, 62}. Consequently, the incorporation of ionic liquids imparts non-volatility and outstanding thermal stability ^{46, 54, 55-59}. Still, a major drawback of these systems is the potential leaching of ionic liquids from the polymer matrix under mechanical stress,

which poses a significant risk to long-term performance. The presence of ion transporters such as water, glycerol, or ILs within the polymer matrix significantly enhances sensor performance. Hydrogel-based polymeric ionic materials, in particular, have demonstrated outstanding results, generating voltages of up to 600–700 mV under loads of 3–20 N (Table 2, entries 12–13) ^{52, 60}, a record among the reported values in Table 2. Notably, neutral hydrogels containing metal salts generally exhibited higher performance (Table 2, entries 11–13) ^{45, 52, 60} compared to polyelectrolyte hydrogels (Table 2, entries 18–22) ^{41, 43-44}. This difference can be attributed to variations in sensor assembly (see section *Operating Parameters*) and the types of ions employed.

Solid polymer electrolytes provide improved safety compared to hydrogels or ionogels, as they eliminate the risks of leakage, evaporation, or leaching associated with liquid phases. The absence of a liquid component is particularly critical for skin- and health-monitoring sensors, ensuring long-term stability, biocompatibility, and reliable performance under continuous wear. These factors have stimulated a growing trend toward the development of solid-state piezoionic sensors (Table 2, entries 23–28) ⁶³⁻⁶⁷. It is particularly important to emphasize the critical role of polymer matrix design in this case. By carefully selecting optimal parameters, such as highly mobile ions, the nature of the polymer backbone, crosslinking density, strong interfacial contact with the electrode material, and the use of elastic electrodes, the solid-state systems can provide strong competition to hydrogels. As seen from the solid-state systems (Table 2, entries 25–26), they can deliver responses of up to 116–190 mV, ranking as the third- and fifth-highest results among all piezoionic sensors reported

Table 2. Polymeric ionic materials and their electromechanical performance in piezoionic sensors.

Entry	Composition of the sensor			Performance of the sensor			Ref
	Polymer matrix	Mobile ions	Electrodes	Generated voltage range (mV)	Applied mechanical stimulus range (kPa, N, %, ° or mm) *	Notes	
Neutral polymers with ionic liquids							
1	PVDF-HFP (55 %wt) ^C	EMIIm ⁺ TFSI ⁻ (37 wt%) ^C	Cu	30 – 90	1.5 – 37.5 kPa	EtMePyrr+ TFSI– was added to the matrix as ionic plastic crystals $\sigma=3.0\times10^{-3}$ S/ cm ⁻¹ ^a Microphase separated ^b Sensor possessed bilayer configuration $\sigma=5.8\times10^{-7}$ S/ cm ⁻¹ ^a Gradient structure ^b	46
2	PVDF-HFP (77 %wt) ^C	EMIIm ⁺ TFSI ⁻ (20 wt%) ^C	Ag nanowires	20 – 95	10 – 60 ° **		54
3	TPU	EMIIm ⁺ TFSI ⁻	RGO/CNT/Ag	0.5 – 2.0	0.3 – 0.7 % **		55
4	TPU	EMIIm ⁺ TFSI ⁻	Graphene	0.5 – 4.5	0.4 – 1.6 % **		56
5	TPU (40 %wt) ^C	U*** (60 %wt) ^C	MXene	210 – 290	0.6 – 1.3 %		57
6	TPU (15.3 %wt) ^C	EMIIm ⁺ TFSI ⁻ (76.1 %wt) ^C	Au/ITO glass	1.0 – 2.5	Max 10 kPa	Lowest detectable pressure was not reported	58



7	TPU (50 %wt) ^C	EMIm ⁺ BF ₄ ⁻ (50 %wt) ^C	MXene/Ag	1.5 – 11	0.3 – 0.7 % **		59
8	TPU	EMIm ⁺ TFSI ⁻	H-reduced graphene oxide (RGO)/carb on nanotubes (CNTs)/Ag	0.6-2.6	0.3 – 1.8 % **		55
Neutral hydrogels with metal salts							
9	PVDF-HFP (95 %wt) ^C	Li ⁺ TFSI ⁻ (5 %wt) ^C	Cu	2.5 – 15	0.2 – 0.8 N	LiTFSI / propylene carbonate solution $\sigma=1.0\times10^{-3}\text{S/ cm}^{-1\text{a}}$	40
10	Crosslinked PAAm	Na ⁺ Cl ⁻	PEDOT:PSS	0 – 0.6	0 – 100 kPa	Crosslinked using methylene bisacrylamide (MBA) and poly (ethylene glycol) diacrylate (PEGDA)	42
11	Crosslinked PAAm/AMPS	Na ⁺ Cl ⁻ K ⁺ Fe[CN] ₆ ³⁻ / K ⁺ Fe[CN] ₆ ⁴⁻	Cu	8 – 150	12.25 – 36.75 kPa	Crosslinked using methylene bisacrylamide (MBA) and poly (ethylene glycol) diacrylate (PEGDA)	45
12	PAAm/PVA (61.6 %wt) ^C	Na ⁺ Cl ⁻ (38.4 %wt) ^C	PEDOT:PSS	6 – 700	1.4 – 20 N	$\sigma=8.00\times10^{-2}\text{S/ cm}^{-1\text{a}}$ Conductive pathways ^b	52
13	Crosslinked PAAm/ PVDF- HFP	Na ⁺ Cl ⁻ Li ⁺ Cl ⁻ Ca ²⁺ Cl ⁻	Cu	4 – 600	3 N	Crosslinked using methylene bisacrylamide (MBA) Porous/microphase separated ^b	60
14	Crosslinked PAAm/AMPS	Li ⁺ Cl ⁻	Au-plated Cu	1.8 – 27.3	30 – 150 kPa	Crosslinked using methylene bisacrylamide (MBA) Gradient Structure ^b	61
Polyelectrolyte ion gels with ionic liquids							
15	Nafion	EMIm ⁺ TFSI ⁻	Au	0.1 – 1.3	0.1 – 1.6 % **		56
16	Nafion	EMIm ⁺ TFSI ⁻	PEDOT:PSS	0.3 – 2.9	0.5 – 3.0 % **	$\sigma=1.4\times10^{-5}\text{S/ cm}^{-1\text{a}}$	62
Polyelectrolyte hydrogels							
17	PAAm-co-PAA (50 %wt) ^C	H ⁺ (50 %wt) ^C	Au	0.4 – 2.8	60 – 350 kPa	15 wt% poly(Acrylic Acid-co- Acrylamide) in DI water (AA:AAm = 50:50)	38
18	Crosslinked PAA (40 %wt) ^C	H ⁺ Li ⁺ Cl ⁻ (59.9 %wt) ^C	Cu	0 – 30	17.4 – 319.16 kPa	Crosslinked using methylene bisacrylamide (MBA)	41
19	Crosslinked gelatin- methacrylate/ PIL	K ⁺	Pt	0 – 35	1 – 50 % 0 – 120 kPa	Crosslinked using methylene bisacrylamide (MBA) $\sigma=4.34\times10^{-4}\text{S/ cm}^{-1\text{a}}$	43
20	Crosslinked gelatin- methacrylate/ PIL	Cl ⁻	Pt	0 – 15	1 – 50 % 0 – 60 kPa	Crosslinked using methylene bisacrylamide (MBA) $\sigma=2.09\times10^{-4}\text{S/ cm}^{-1\text{a}}$	43
21	Crosslinked PAAm/PIL (23.1 %wt) ^C	K ⁺ (76.9 %wt) ^C	Pt	0 – 70	1 – 22.5 kPa	Crosslinked using methylene bisacrylamide (MBA) $\sigma=1.05\times10^{-3}\text{S/ cm}^{-1\text{a}}$ Gradient Structure ^b	44
22	Crosslinked PAAm/PIL (26.5p %wt) ^C	Cl ⁻ (73.7 %wt) ^C	Pt	0 – 70	1 – 22.5 kPa	Crosslinked using methylene bisacrylamide (MBA) $\sigma=7.11\times10^{-4}\text{S/ cm}^{-1\text{a}}$ Gradient Structure ^b	44
Solid-state polyelectrolytes							
23	Nafion	H ⁺	Au	1.5 – 3.5	0.5 – 1.4 % **		63
24	Nafion	H ⁺	Au	25 – 40	1.0 – 1.6 % **	Au electrode was deposited on polymer with specific technology allowing for the	64

formation of fused tree-root-like structures. View Article Online
DOI: 10.1039/D5MH01784J

25	Nafion	H ⁺	Graphdiyne	28 – 116	0.2 – 0.8 % **	The ultrafast out-of-plane ion transfer was facilitated by the triangular pores in the graphdiyne electrodes	65
26	PIL (5 %wt) ^c	BMIIm ⁺ (75 %wt) ^c	Pt	0.7 – 190.3	1 – 80 kPa	Crosslinked PIL $\sigma = 1.7 \times 10^{-6} \text{ S/cm}^{-1 \text{ a}}$	66
27	PIL (5 %wt) ^c	TFSI ⁻ (75 %wt) ^c	Pt	7.0 – 29.5	1 – 80 kPa	Crosslinked PIL $\sigma = 9.6 \times 10^{-7} \text{ S/cm}^{-1 \text{ a}}$	66
28	PEO/PIL (60 %wt) ^c	TFSI ⁻ (40 %wt) ^c	PEDOT:PSS	0.1 – 0.4	0.2 – 1 mm **	Ionic semi-interpenetrated network was used as matrix $\sigma = 8.7 \times 10^{-5} \text{ S/cm}^{-1 \text{ a}}$	67

* Mechanical stimulus is either pressure in kPa, force in N, strain in %, bending angle in ° or displacement in mm.
** Piezoionic sensors were tested in bending configuration.
*** Ionic liquid unspecified.
^a Ionic conductivity at 25°C for some reported materials
^b Morphological features
^c Chemical composition of the top-performing piezoionic sensor (ionic moiety and neutral backbone weight %)

4. Ion mobility

Ion mobility depends on the diffusion of ions within the matrix, which in turn depends on the ion's electronic charge, ion size, ion concentration, and electrophoretic mobility^{38-39, 44}. According to the Stokes-Einstein equation (eq. 9), where D_i is the diffusion coefficient of ion i , κ_b is the Boltzmann constant, T is the absolute temperature, η is the viscosity, and r_i is the hydrodynamic radius of the ion,⁷¹ larger ions would experience higher viscous drag force, thus decreasing the diffusion of ions within the direction of the fluid flow as follows:

$$D_i = \frac{\kappa_b T}{6\pi\eta r_i} \quad (\text{eq. 9})$$

This difference is well illustrated by comparing TPU-based systems incorporating EMIm⁺TFSI⁻^{55-56, 58} and EMIm⁺BF₄⁻⁵⁹ ionic liquids (Table 2, entries 3-4, 6 and 7). While the cation remains the same, the BF₄⁻ anion is considerably smaller than TFSI⁻, which enables higher ion mobility and, consequently, improved sensor performance. According to the Nernst-Einstein equation (eq. 10) where μ_{qi} is ionic mobility of ion i , D_i is the diffusion coefficient of ion i , κ_b is the Boltzmann constant, T is the absolute temperature, z_i is the electron valence of ion i , e is the fundamental charge⁷¹, the migration of ions is also under the influence of a transient electrical field during charge separation, referred as the electrophoretic mobility, reducing the ion transport within the direction of the fluid flow as follows:

$$\mu_{qi} = \frac{q_i D_i}{\kappa_b T} = \frac{z_i e D_i}{\kappa_b T} \quad (\text{eq. 10})$$

Although ion-matrix, ion-ion, and ion-solvent interactions are not considered, the combination of eq 9. and eq. 10 leads to eq. 11, showing that the charge to ion size ratio clearly defines the ionic mobility⁷¹.

$$\mu_{qi} = \frac{z_i e}{6\pi\eta r_i} \quad (\text{eq. 11})$$

As a result, the total migration flux of an ion is mainly due to the convection flow whereas the viscous flow (with respect to concentration gradient; diffusive flow) and the electrophoretic flow (with respect to the charge gradient) drive the migration of ions in a reverse direction, causing voltage decay³⁸.

5. Material dimensions

Material dimensions like the material thickness affect the pressure distribution along the polymeric matrix. Specifically, the lower the material thickness, the higher the generated voltage and the response speed with respect to narrow force distribution upon mechanical deformation^{38, 45-46}. Therein, poroelasticity describes the time-dependent behavior of fluid-containing materials during mechanical loading³⁸. Under mechanical stimulation, the ions transport with the fluid flow due to pressure gradient generation, which subsides and redistributes within the material until the pressure is equilibrated. The characteristic time taking for a material to relax after a deformation is applied, namely the poroelastic relaxation time as expressed by $\tau = \frac{(1-2\nu)\eta L^2}{2(1-\nu)G\kappa} \sim \frac{L^2}{D}$, where L is the characteristic length, ν is the poisson's ratio, G is the modulus, η is the fluid viscosity, κ is the material permeability and D is the effective diffusivity of the fluid, govern the piezoionic recovery time^{38, 72-73}. As a result, longer poroelastic relaxation time, results in slower fluid flow, which in turn leads to longer recovery times⁷²⁻⁷³.

6. Charge density, crosslinking density and material density

These are key parameters affecting the charge separation and the resulting output voltage with respect to the flow of charges within the material. Charge density herein refers to the amount of mobile ions (or charge) per unit of volume, so that the higher the charge density, the higher the generated output voltage. In contrast, the crosslinking density corresponds to the degree of crosslink points per unit in volume, leading to higher resistance to flow within the material. Therein, the generated output voltage amplitude at a given applied pressure is approximately proportional to the charge density and inversely proportional to the crosslinking density⁴⁴. Dobashi *et al.*³⁸ attributed a slight attenuation of the output voltage amplitude together with longer recovery time to the material density, namely the mass of a material per unit of volume. The latter more formally leads to changes in the material permeability (ability for fluids to flow through the media) and stiffness (modulus)³⁸⁻³⁹.



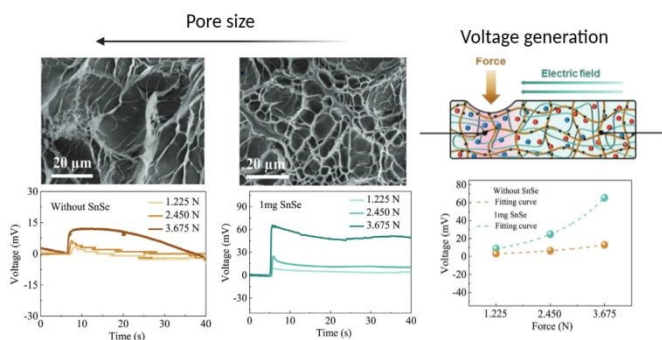


Fig. 5. Influence of porosity upon addition of Tin Selenide nanosheets (SnSe) within polymeric ionic materials with respect to higher generated output voltage. Adapted under terms of the CC-BY license with permission⁴⁵; © 2023 Wiley-VCH GmbH.

Novel strategies for structural design towards enhanced piezoionic performance

Recently, several novel structural design strategies have been proposed to enhance the performance of piezoionic sensors. These include the introduction of porosity, microphase separation, gradient-like architectures, and the creation of conductive pathways or gates as follow:

7. Porosity

Porosity refers to the ratio of void space inside the total volume in a material, generally obtained by means of solvent casting or porogen leaching^{60, 74}. Porosity directly influences the mechanical properties (stiffness) and permeability of the material, which govern the ion diffusion within the piezoionic material (**Fig. 5**)^{38, 45, 60}. Accordingly, porosity enhances the generated output voltage through two main mechanisms: (1) facilitating easier deformation (reduced stiffness), which increases electromechanical sensitivity, and (2) enhancing the dipole moment, which promotes more efficient charge separation^{45, 60}. Using double-network nanocomposites embedded with an electrolyte (NaCl or $K_3Fe(CN)_6/K_4Fe(CN)_6$), Li *et al.*⁴⁵ demonstrated that smaller pore sizes lead to larger mobility difference between the ions, thus allowing higher output voltage. Lu *et al.*⁶⁰ further demonstrated a three-fold increase in the output voltage (up to 14 mV under 3 N loading) from porous PAAm hydrogels embedded with electrolytes ($CaCl_2$, NaCl or LiCl) compared to the nonporous counterparts together with higher output voltage with respect to the hydrated ion sizes: Ca^{2+} (4.12 Å) > Li^+ (3.82 Å) > Na^+ (3.58 Å) due to higher mobility imbalance (Table 2, entries 11, 13).

8. Microphase separation

Microphase separation is a phenomenon in which a materials organizes into distinct domains⁷⁵. This structural arrangement enables higher output voltage amplitudes under increased pressure gradients by concentrating stress within the hard phases, while simultaneously exploiting the high ionic mobility of the soft and intermediate phases (**Fig. 6**)^{46, 60}. Therein, Lu *et al.*⁶⁰ combined microscopic porosity and hydrophilic-hydrophobic phase separation into electrolyte-loaded PAAm networks for prominent piezoionic performance, generating output voltages as high as 600 mV in response to medical ultrasound stimulation (Table 2, entry 13).

Besides, Zhu Weiyan *et al.*⁴⁶ introduced EMIm⁺TFSI⁻ ionic liquid as a compatibilizer within a microphase-separated system based on ionic plastic crystals and PVDF-HFP for stress concentration and localized charge separation, yielding better mechanical properties and effective voltage generation up to 90 mV under a 15 kPa loading.

9. Gradient-like structures

Gradient-like structures refer to materials with gradually varying properties along their volume (**Fig. 7**)⁷⁶. Odent *et al.*⁴⁴ developed such polyelectrolyte hydrogels through copolymerization of AAm with either anionic 3-sulfopropyl acrylate potassium salt (SPA) or cationic [2-(acryloyloxy)ethyl]trimethylammonium chloride (AETA) co-monomers (Table 2, entries 20-21). This was achieved using stereolithography 3D printing of stacked ionic assemblies composed of discrete compartments with distinct ion transport properties. By varying the ion type, charge density, and crosslinking density across these compartments, the output voltage magnitude and polarity of the resulting piezoionic device could be precisely programmed (**Fig. 7. A**). The generated voltage at a given applied pressure was found to be directly proportional to the hydrogel's charge density and inversely proportional to its crosslinking density. Gradient-like structures leverage this principle and allow to program signal magnitude, enabling controlled amplification or attenuation, through the flow of excess charges from the indented compartment to adjacent compartments with different ion transport properties. In this way, the resulting touch sensors can be integrated onto fingertips to enable the tactile perception for object recognition applications. Recently, Li *et al.*⁶¹ dramatically enhanced the piezoionic outputs of LiCl-embedded PAAm hydrogels by the synergistic effects between geometry, modulus (stiffness), and charge gradients (Table 2, entry 14). While the geometry and modulus gradients enhance the pressure gradient generation, the charge gradient increases the mobility difference between the ions, thus leading to higher output voltage (**Fig. 7. B**). Similarly, Kim *et al.*⁵⁴ (Table 2, entry 2) developed a bilayer-structured polymeric ionic materials that exhibited a significantly enhanced output signal and faster response time due the presence of an ion accumulation interface (**Fig. 7. C**). The material further demonstrated the capability

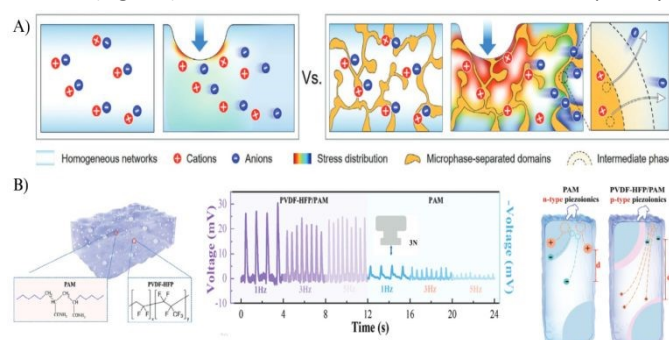


Fig. 6. Influence of microphase separation within polymeric ionic materials with respect to higher stress localization and enhanced ion separation in comparison to homogeneous networks (A). Microphase separated PAAm/PVDF-HFP leads to higher transient voltage generation compared to homogeneous PAAm network with respect to higher ion mobility difference (B). Adapted under terms of the CC-BY license with permission^{46, 60}; © 2023-2024 Wiley-VCH GmbH.



REVIEW

Materials Horizons

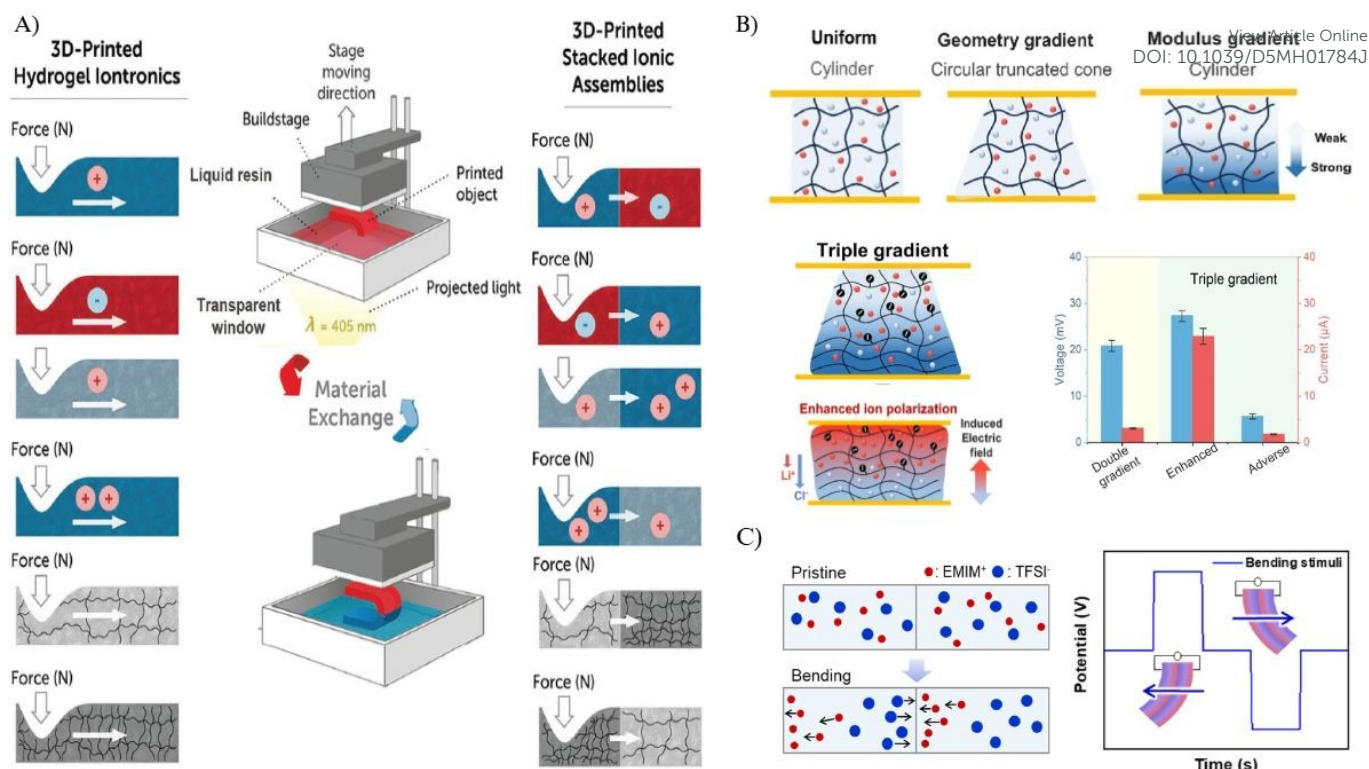


Fig. 7. Gradient-like structures by means of variations in ion type, charge density, and crosslinking density within the piezoionic device via resin vat exchange during 3D printing (A). Reproduced under terms of the CC-BY license with permission⁴⁴; © 2022 Wiley-VCH GmbH. Synergy effects of geometry, modulus (stiffness), and charge gradients in voltage generation (B). Bilayer polymeric ionic materials with enhanced piezoionic performance with respect to an ion accumulation interface (C). Reproduced under terms of the CC-BY license with permission^{54, 61}; Copyright Elsevier © 2024-2025.

to accurately detect both static and dynamic forces, including specific motions such as bending and vibrations.

10. Conductive pathways and gates

Conductive pathways and gates enable to boost the transport of ions within the material, thus improving the piezoionic performance. Dai *et al.*⁴¹ (Table 2, entry 18) introduced oriented polyethylene terephthalate (PET) fibers into LiCl-embedded polyacrylic acid to create conductive pathways that facilitate ion transport along the negatively charged fiber surfaces (Fig. 8). As a result, the output voltage measured parallel to the fiber orientation was significantly higher (27.5 mV vs. 4.3 mV under a 290 kPa load) and exhibited a much faster recovery time (1.5 s vs. 30 s) compared to the perpendicular direction. Wang *et al.*⁵² (Table 2, entry 12) employed a combination of PAAm, polyvinyl alcohol (PVA), and poly(3,4-ethylenedioxythiophene):poly(styrenesulfonate) (PEDOT:PSS) followed by a simple dry-annealing process to induce a gating effect. Under high pressure, this effect results in the accumulation of anions within the indented region. The resulting gate remains open under low deformation, but progressively closes once a threshold force is exceeded. Mechanistically, PEDOT forms crystalline aggregates through π - π stacking, which undergo oxidation to create a conductive polymer network. This network contains excess positive charges (holes) that electrostatically interact with anions embedded in the hydrogel, thereby reducing their diffusivity⁵². In contrast, PSS with its negatively charged sulfonate groups forms ordered nanostructures acting as pathways for embedded cations to move within the hydrogel⁵².

Unveiling operating parameters on piezoionic voltage generation

Operating parameters associated with sensor configuration and assembly can significantly influence fluid-driven ion transport in piezoionic sensors (see Fig. 9). In the following, we examine in detail the most critical of these parameters:

Electrode configuration

The two-electrode configuration is the most widely adopted assembly scheme for piezoionic sensors, typically implemented in two modes: coplanar and bending. In the coplanar mode, two electrodes are positioned on the same surface of the material, which is subjected to a compressive stimulus. This drives ion flow and charge transport perpendicular to the indentation. When the reference (ground) electrode is placed beneath the indented region and the working (sense) electrode on the undeformed region, the resulting voltage polarity can be interpreted based on the ion species preferentially displaced: a positive output indicates cation-driven transport, whereas a negative output indicates anion-driven transport (and vice versa)⁴⁴. By contrast, electrodes are placed on opposite faces of the material in the bending mode, where bending deformation drives ion flow and charge transport parallel to the deformation. Although, Ko *et al.*⁵⁴ suggested a bilayer-structured ionic materials to enhance the output signal and the response time of the sensor, where after spraying of the silver nanowires on one

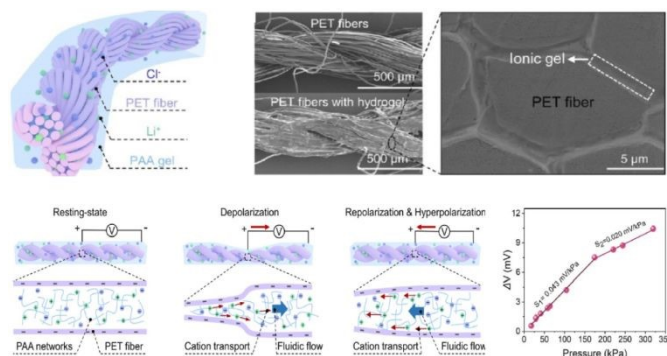


Fig. 8. Conductive pathways by oriented PET fibers within piezoionic materials, providing higher mechanical-to-ionic transduction and resulting voltage generation along the fiber directions. Reproduced under terms of the CC-BY license with permission⁴¹; Copyright Elsevier © 2024.

side of the film and half-cutting, the two films were assembled face-to-face (Table 2, entry 2).

Electrode composition

Various electrode materials were investigated (Table 2), including metal electrodes such as Cu^{40-41, 45, 60}, Au^{38, 62-64}, Ag⁵⁴ and Pt⁶⁶, reduced graphene oxide/carbon nanotubes/silver (RGO/CNT/Ag)⁵⁵, gold and Indium tin oxide glass (Au/ITO glass)⁵⁹, graphene⁵⁶, two-dimensional titanium carbide/silver (MXene/Ag)⁵⁷ and PEDOT:PSS^{52,67}. The wide range of electrode material choices stems from some challenges related to contact with elastic polymer films or hydrogels and precise current collection. Vapor-phase deposition is primarily employed for sensors operating in compression mode, where a thin conductive layer, typically noble metals, is directly coated onto polymer films or ionogels, providing excellent conductivity and signal retention^{55, 62-63, 66}. Although noble metals have been widely used as electrodes, their poor mechanical compliance and limited stability under high deformation significantly restrict their effectiveness in bending-mode sensors, especially under large strains^{55, 62, 77-78}. In bending mode, electrode selection plays a more decisive role in determining the generated voltage, largely due to interfacial challenges between polymeric ionic materials and electrodes^{55, 56, 58, 63-64}. To overcome these limitations, more flexible and conductive alternatives such as Ag nanowires⁵⁴, graphene⁵⁶, MXene^{57, 59}, graphdiyne⁶⁵, and PEDOT:PSS^{42, 52, 62, 67} have been investigated (Table 2, entries 2, 4, 5, 7, 10, 12, 16, 25, 28). For instance, Lu *et al.*⁵⁶ (Table 2, entry 5) developed a trilayer sensor based on TPU matrix with ILs and MXene electrodes, demonstrating superior electromechanical transduction. The improved performance was attributed to ultrathin MXene layers with larger surface area and higher pore distribution compared to bulk MXene, yielding output voltages up to 219 mV with excellent cycling stability (98 % retention after 10,000 cycles). In another study, Lu *et al.*⁶⁵ (Table 2, entry 25) reported a trilayer sensor composed of Nafion and graphdiyne electrodes, which facilitated rapid in-plane and out-of-plane ion transport. This design achieved a high output voltage of 116 mV along with robust stability (94.7 % signal retention after 4000 cycles). Similarly, conductive polymers such as PEDOT:PSS impart stability, high conductivity, and excellent stretchability to polymeric sensors^{42, 52, 57}. For example, Ribeiro *et al.*⁶⁷ (Table 2, entry 28)

fabricated highly stretchable, ionically conductive films coated with flexible PEDOT:PSS electrodes on both sides. At low scan rates, these devices demonstrated volumetric capacitances equivalent to, or even exceeding, those systems employing ionic liquid electrolytes.

Electrode distance

Electrode spacing strongly influences both output voltage magnitude and recovery time, as it determines the spatio-temporal variation of fluid flow that drives ion transport³⁹. Under mechanical stimulation, a pressure gradient induces fluid flow, which carries ions and establishes a spatio-temporal electric field within the piezoionic device. Therein, Xu *et al.*³⁹ systematically investigated the effect of the electrode distance using both cationic and anionic single-ion based piezoionic sensors. They demonstrated that increasing the electrode distance leads to higher output voltages but also results in longer recovery times (Fig. 10). This behaviour can be explained by the spatial dependence of the electrical potential, described as $V = \int E(x,t)dx$, where V is the voltage, E is the electrical field, x is the distance between the electrodes and t is time. Accordingly, a larger electrode distance results in a higher output voltage. In contrast, the higher the electrode distance, the higher the recovery time as a longer poroelastic relaxation pathway is required for the material to fully recover after deformation³⁹.

Indentation size and speed

Indentation size and speed play a crucial role in pressure gradient generation during mechanical loading. Larger indentation sizes result in higher voltage outputs⁴⁴. Apart, Xu *et al.*³⁹ showed that increasing indentation speed enhances both output voltage and reduces recovery time. However, the voltage response eventually saturates at high indentation speeds, reaching a plateau that reflects an optimal characteristic fluid flow velocity³⁹. Similarly, the response

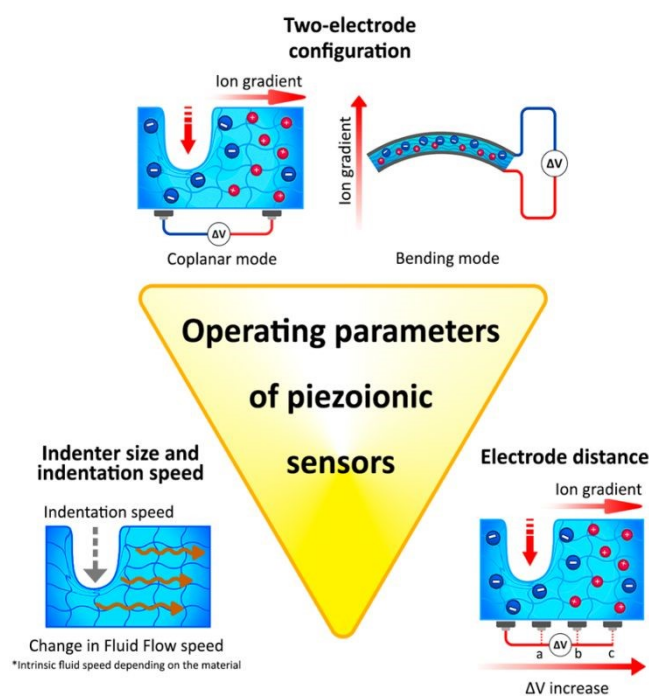


Fig. 9. Operating parameters affecting the fluid-driven ion transport and voltage generation in piezoionic sensors, including the electrode configuration, the electrode distance and the indentation characteristic (size and speed).



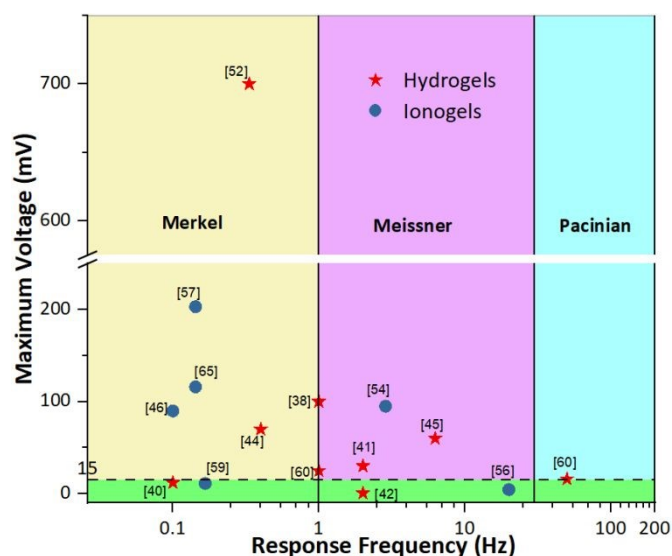


Fig. 11. Maximum voltage with respect to frequency response time of common polymeric ionic materials. Range of action potential (green region), frequency range of Merkel cell (yellow region), frequency range of Meissner Corpuscles (purple region) and frequency range of Pacinian Corpuscles (teal region) are identified.

and recovery times (FWHM) reaches a plateau with further increases in indentation speed. Consistently, Dai *et al.*⁴¹ reported a comparable trend, observing increased output voltage with faster indentation speeds.

Applications

Soft wearable electronics are increasingly being employed for continuous, non-invasive health monitoring of physiological parameters, offering improved disease diagnosis, progression tracking, and treatment at a relatively low cost⁷⁹⁻⁸⁰. The latter typically consist of a sensing unit combined with a data collection/transmission unit and a power supply⁸¹. Piezoionic systems are self-powered and highly sensitive to mechanical stimuli, making them suitable for telehealth applications. This requires the detection of subtle signals and continuous monitoring over extended periods, such as the case of cardiac monitoring⁶⁵. For example, cardiovascular monitoring, including heart rate and blood pressure monitoring, is crucial for the early detection of heart conditions and diseases⁶⁵. In this regard, piezoionic sensors readily allow the continuous monitoring of the patient deterioration⁷⁹⁻⁸⁰. Lu *et al.*⁶⁵ developed a wearable piezoionic sensor capable of distinguishing between systolic and diastolic blood pressure, with measurements consistent with those of commercial devices. Ma *et al.*⁴² introduced a dual piezoionic sensor to monitor both the heart rate and sodium levels in sweat to provide heart parameter monitoring and homeostasis information. While others reported on piezoionic sensors for monitoring heart rate, blood pressure, and human motion^{56-57, 65}, they have been also used for respiratory and sleep monitoring^{56-57, 65}.

Ionic skins, tissue engineering, and biointerfaces represent a promising avenue of applications for piezoionic sensors with respect to their biomimetic mechanical-to-ionic transduction mechanism, mimicking biological signal production and transmission⁶⁻⁸. Particularly, the complex tactile perception gave rise to the

development of ionic-based systems able to mimic some of the functionalities of the skin, well-known as ionic skin^{82,83}. Wang *et al.*⁸² developed a piezoionic material able to discriminate between innocuous and harmful touch similarly to the skin receptors. Lu *et al.*⁶⁰ develop a piezoionic sensor able to differentiate pressure spatial localization. Tissue engineering is an interdisciplinary field that focuses on the restoration of damaged or diseased tissues, requiring biocompatible materials which allow cell attachment, proliferation, and differentiation. Therein, Burattini *et al.*⁴³ proved the biocompatibility of gelatin-based single-ion piezoionic systems with respect to cell proliferation and differentiation of myoblast with no adverse effect. Biointerfaces are devices that interact with the neural system to treat a disorder or symptom^{81,83}. In that regard, Dobashi *et al.*³⁸ demonstrated the neuromodulation capabilities in mice of piezoionic system able to elicit muscle excitation. Lue *et al.*⁴¹ developed an artificial nerve system using a composite of PET microfiber and PAAC hydrogel, which neuromodulated stimuli in mice peripheral sciatic nerve. This proves its capabilities to communicate and be integrated with biological nerve systems. In general, polymeric ionic materials to be of use either for ionic skin, biointerfaces, neuromodulation or neuroprosthetics must generate an electrical potential of approximately 15-20 mV (threshold potential) to trigger an action potential, enabling communication within the body^{6-10, 38, 41}. Focusing on ionic skin applications, piezoionics materials should be able to mimic the complex somatosensory system of the skin. Specifically, mimicking the four low-threshold mechanoreceptors in the skin: Merkel cells, Meissner corpuscles, Pacinian corpuscles, and Ruffini ending. Firstly, polymeric ionic materials sensitivity to deformation should match the sensitivity of these mechanoreceptors in the skin, which can detect forces as subtle as 0.5 mN⁶⁻⁸. As such, **Fig. 11** illustrates the maximum output potential against the frequency response time for selected piezoionic sensors. Most current piezoionic systems exhibit frequency responses similar to those of Merkel cells and Meissner corpuscles, with maximum potentials exceeding 15 mV rendering them able to trigger an action potential. Thus, they could be used for neuromodulation, ionic skin or biointerfaces. Nonetheless, piezoionic systems with a frequency response similar to that of Pacinian Corpuscles are still missing. The development of piezoionic systems capable of mimicking each type of mechanoreceptor is a step toward producing more complex ionic skin able to fully mimic the intricate touch perception of skin.

Energy harvesting appears as a promising application for piezoionics owing to their ability to convert mechanical energy into electrical energy⁴⁸. Yet, piezoionic devices are less efficient than common energy harvesters with respect to the production of low output voltage in the few hundreds millivolts, with only a peak power per volume being comparable to that of common harvesters^{38, 52, 60}. While piezoelectric devices produce a power density in the range of 0.4-30 $\mu\text{W}/\text{cm}^3$ ⁸⁴. In contrast, piezoionics are reported with power density in the range of 0.85-1.3 $\mu\text{W}/\text{cm}^3$ ^{38, 52, 60}. Despite these limitations, piezoionic systems offer substantial potential for further improvement and are competitive with some low performance piezoelectric harvesters. Yet, the mechanical-to-ionic transduction is

relatively novel and has not been extensively studied, especially as energy harvesters, suggesting a promising avenue for enhancing its capabilities as next-generation energy harvesters.

Limitations for real-sensing devices persist as several challenges must still be overcome before piezoionic transducers can be translated into practical and reliable sensing technologies. These constraints such as a slower response impact the device performance, depending on the specific application. In this regard, overcoming these limitations is the cornerstone for achieving functional integration and ensuring long-term operational stability in real world sensing environments. The strategies that are previously developed to mitigate these limitations in the realm of soft sensor technologies afford promising avenues for future adaptation in piezoionic device as described hereafter^{85–86}. A primary limitation stems from the intrinsic water-dependent behaviour of piezoionic transducers, which can be mitigated through encapsulation strategies for minimizing water loss and enhancing environmental stability³⁸. However, the encapsulation must be judiciously designed to preserve mechanical compliance, maintain ionic conductivity, and ensure long-term durability. This consideration is particularly critical for ionic-skin applications, where the mechanical properties of the device must closely match those of biological tissues. An alternative approach consists to the development of water-retaining materials^{87–88} that demonstrate remarkable stability under extreme temperature variations, thereby enabling reliable device performance through diverse environmental conditions. Aside from encapsulation and the development of water-retaining materials, deep eutectic solvent-based systems have emerged as a promising alternative for ionic skins, offering superior properties than regular ionogels⁸⁹. The implementation of all-solid-state systems represents another promising approach, offering liquid-free materials with moderate ionic conductivity, robust mechanical properties, and high thermal stability. As demonstrated by Ribeiro *et al.*⁶⁷ whom reported a PIL-based piezoionic sensor, such materials exhibit exceptional compatibility for achieving stable piezoionic performance. The absence of liquids (*e.g.* water) can mitigate dehydration and leakage, substantially extending device operational lifetime. Being particularly relevant to ionic-skin, tissue-engineering, and biointerfaces applications, stringent biocompatibility requirements can severely constrain the selection of suitable materials that can be safely interfaced with tissues^{81,85}. While piezoionic transducers possess tissue-like mechanical softness and ionic transport characteristics comparable to those of biological tissues, their stable operation under physiological conditions remains challenging due to the dehydration, leaching, and compositional instability. Achieving robust adhesion and seamless integration with biological systems, without perturbing native physiological functions, also constitute a major frontier for these applications^{49,85}. Beyond hydration stability and biocompatibility, ensuring durability and long-term operational reliability certainly represent another crucial design objective⁸⁵. Being subjected to repeated mechanical and environmental stresses, soft electromechanical sensors can underscore the need for resilient, self-healing materials to support the realization of stable, long-lasting sensing platforms. For instance, the incorporation of

reversible bonding interactions (similarly to supramolecular materials) can substantially enhance durability, improve mechanical performance, and extend the overall device lifespan⁹⁰. For example, Hu *et al.*⁹¹ developed a supramolecular ionic gel with self-healing capability for soft sensor applications based on deep eutectic solvent, while Kim *et al.*⁵⁴ reported a piezoionic sensor (PVDF swollen in EMIM-TFSI) integrating similar autonomous self-healing functionality. Both response and recovery times are key determinants of piezoionic device performance. They are influenced by mechanical hysteresis stemming from viscoelastic energy dissipation⁹² and ionic hysteresis arising from the temporal mismatch between pressure-driven ion transport and diffusion-mediated re-equilibration^{38,49}. Although piezoionic transducers typically exhibit response and recovery times on the order of seconds suitable for soft wearable electronics, mechanical hysteresis continues to pose a significant challenge. In particular, low mechanical hysteresis is an imperative characteristic for soft sensor, facilitating the swift recovery of deformed materials, swift electrical signal response, and the maintenance of signal cyclic stability⁹³. Among strategies to reduce mechanical hysteresis, supramolecular architectures can distribute stress uniformly under repeated deformation, minimizing energy dissipation^{92,94}. For example, Sun *et al.*⁹⁴ reported a low-hysteresis supramolecular ionogels achieving *ca.* 11.7% hysteresis at 400% strain. Other strategies to reduce mechanical hysteresis include densely entangled polymer networks, phase separation, or the incorporation of controlled microstructures such as microcracks and microchannels, which guide deformation and facilitate recovery to the original shape^{86,92}. To date, piezoionic devices for energy harvesting and biointerfaces applications must require rapid response and recovery, making ionic hysteresis a critical challenge. Conductive pathways, as demonstrated by Dai *et al.*⁴⁹, endow faster response and recovery times. For biointerfaces, particularly in neuromodulation, the stimulation frequencies of the device is crucial for achieving therapeutic efficacy (as determined by the response and recovery times)⁹⁵. For energy harvesters, slow mechanical-to-ionic transduction limits operational frequency, restricting energy conversion efficiency compared with conventional electromechanical sensors. Therein, structural design strategies including gradient-like structures, controlled porosity, and microphase separation can enhance output voltages and efficiency. A careful attention to data acquisition, calibration, and signal processing is essential as piezoionic transducers are sensitive to external noise, including capacitive and triboelectric interferences³⁸. Ultimately, the convergence of these advances will enable piezoionic devices that are stable, reproducible, and fully compatible with the mechanical and operational demands of next-generation applications.

Conclusions

Polymeric ionic materials undoubtedly represent the base of next-generation ionic-electromechanical sensors with respect to their biomimetic mechanical-to-ionic transduction mechanism, mimicking biological signal production and transmission. Overall, a



REVIEW

Materials Horizons

fluid pressure gradient is created under mechanical stimulation which drives fluid flow within the matrix. As a result, a transient separation between cations and anions takes place due to their different mobilities and interaction, breaking electrical neutrality and generating a transient voltage. Although the working principle of the mechanical-to-ionic transduction in polymeric ionic materials is not yet fully understood, a foundational framework has been established that outlines the underlying transduction mechanism and the key parameters governing voltage generation.

We classified these parameters into two groups based on their principle of action: **structural parameters** primarily relate to the design of the polymer matrix, while **operational parameters** concern sensor assembly and practical operation. Among the structural parameters, the most critical ones are the type of polymer matrix, the nature and mobility of the ionic species, the conduction mechanism (single-ion vs. ion-pair), material dimensions (including thickness), charge density, crosslinking density, porosity, microphase separation, as well as the presence of gradient-like structures or conductive pathways. The performance of piezoionic sensors is strongly governed by the type of polymer matrix and the mobility of the incorporated ionic species. While hydrogel- and ionogel-based systems offer exceptionally high voltage outputs due to the presence of liquid ion transporters, their long-term stability is limited by evaporation, leakage, or leaching. In contrast, solid-state polyelectrolyte systems eliminate these drawbacks, providing superior safety, durability, and suitability for skin- and health-monitoring applications. Importantly, single-ion conducting solid-state matrices, particularly those based on polyelectrolytes and poly(ionic liquid)s, are the most promising direction, as they enable stable ion-gradient formation, reduced voltage decay, and competitive output voltages (up to 190 mV). Ion mobility is governed by ion diffusion within the matrix, which is influenced by factors such as ionic charge, size, concentration, and electrophoretic mobility. In single-ion conducting systems, optimal performance is achieved when the mobile ions are small, exhibit high charge delocalization, and show minimal coordination with the polymer matrix. By contrast, in ion-pair conducting systems, performance can be enhanced by selectively reducing the mobility of one ionic species, thereby facilitating the formation of stable charge gradients.

Thinner films are more favorable, as they enable higher voltage generation and faster response due to narrower force distribution and shorter poroelastic relaxation times. A high charge density is critical, since a greater number of mobile ions per unit volume directly amplifies the generated output voltage. In contrast, the crosslinking density should be kept relatively low, because excessive crosslinking restricts fluid and ion transport, leading to reduced voltage output and slower response. A moderate degree may still be required to maintain mechanical robustness. Lower material density is preferable, as high density increases stiffness and reduces permeability, which slows fluid flow and extends recovery times. Overall, the most promising polymer matrices for piezoionic sensors are therefore thin, lightweight, and moderately crosslinked systems with high charge density. Such a combination maximizes ion

transport efficiency, enhances voltage generation, and ensures fast response and recovery times under mechanical loading.

When speaking about additional structural design, the highest-performing piezoionic polymer matrices based on ion-pair mobility should combine small, well-distributed porosity and microphase-separated domains. An optimal porous structure is beneficial, as it reduces stiffness (enhancing electromechanical sensitivity) and increases charge separation efficiency. Smaller, well-distributed pores are especially effective, since they maximize ion mobility differences and improve voltage generation. The coexistence of hard and soft domains allows stress concentration in rigid phases while enabling rapid ion transport in soft regions. For both single-ion and ion-paired systems, the creation of gradient-like architectures and the incorporation of directed conductive pathways and gating mechanisms are of great importance. By designing gradients in ion type, charge density, stiffness, or geometry, the system can achieve controlled amplification, faster responses, and multifunctional sensing capabilities such as discrimination between static and dynamic forces.

As the mechanical-to-ionic transduction is relatively new and not yet extensively studied, there is currently no standardized approach to assembling and testing piezoionic sensors. Different authors employ diverse evaluation methods, making direct comparison of results challenging. While most studies report the generated voltage under varying mechanical loads, data on relaxation time (how quickly the sensor can be reused without loss of sensitivity) and response time (how rapidly it responds to an applied load) are generally lacking. Despite these limitations, this review not only provides guidelines for designing efficient piezoionic devices with enhanced performance but also outlines optimal strategies for sensor assembly and offers fundamental insights into the underlying piezoionic mechanism. Ultimately, careful matrix design via optimization of ionic mobility, crosslinking density, and electrode interfaces, will be essential to advancing solid-state piezoionic sensors as the leading platform for future applications.

Author contributions

Conceptualization: J.A.G., C.P., J.-M.R., J.O. ; Investigation: J.A.G., V.S. ; Supervision: J.-M.R., J.O. ; Writing – original draft: J.A.G., J.O. ; writing - review and editing: C.P., A.S., J.-M.R., J.O. ; funding acquisition: A.S., J.-M.R., J.O.. All authors have read and agreed to the published version of the manuscript.

Conflicts of interest

There are no conflicts to declare.

Acknowledgements

We gratefully acknowledge support from the Belgian Federal Government Office of Science Policy (SSTC-PAI 6/27) as well as both Wallonia and the European Commission "FSE and FEDER". The authors acknowledge the PDR project "INFINITE" with the financial support of the Fonds de la Recherche Scientifique (F.R.S.-FNRS) and the Luxembourg National Research Fund (FNR) (agreement number



INTER/FNRS/21/16555380/INFINITE). J.-M.R. is a FNRS Research Director and a WEL-T Researcher.

Notes and references

- Cao, R., Tian, H., Tian, Y., & Fu, X. *Advanced Science*, 2024, **11**(11), 2302327.
- Liu, S., Wang, S., Zou, L., & Xiong, W.. *Cellular and Molecular Life Sciences*, 2021, **78**, 5083-5094.
- S. Maksimovic, M. Nakatani, Y. Baba, A. M. Nelson, K. L. Marshall, S. A. Wellnitz, P. Firozi, S.-H. Woo, S. Ranade, A. Patapoutian and E. A. Lumpkin, *Nature*, 2014, **509**, 617–621
- M. J. Caterina, *J. Clin. Invest.*, 2021, **131**, e1565871
- D. Julius, *Annu. Rev. Cell Dev. Biol.*, 2013, **29**, 355–384
- Yamada, A., Ling, J., Yamada, A. I., Furue, H., & Gu, J. G. *Neuron*, 2024, **112**(8), 1286-1301.
- Wang, L., Ma, L., Yang, J., & Wu, J, *Cyborg and Bionic Systems*, 2021
- Roe, A., Friedman, R. & Chen, L. in *Handbook of Neurochemistry and Molecular Neurobiology: Sensory Neurochemistry* (eds Johnson, D. A. & Lajtha, A.) 1–16
- Xiao, K., Wan, C., Jiang, L., Chen, X., & Antonietti, M. , *Advanced Materials*, 2020, **32**(31), 2000218.
- Sun, G., Wang, P., Jiang, Y., Sun, H., Meng, C., & Guo, S., *Soft Science*, 2022, **2**(4).
- Ha, K. H., Huh, H., Li, Z., & Lu, N , *ACS nano*, 2022, **16**(3), 3442-3448
- Hu, Jianguo, Guanhua Dun, Xiangshun Geng, Jing Chen, Xiaoming Wu, and Tian-Ling Ren, *Nanoscale Advances* 5, 2023, **12**, 3131-3145.
- Zhang, Z. *SHS Web of Conferences*, 2023, **157**, 01026.
- Zhang, X., Xu, J., Chen, Z., Zhu, G., Wei, A., & Chen, D. *Journal of Alloys and Compounds*, 2024, **1007**, 176408.
- Chen, J., Song, T., Wang, X., Zhou, Y., Wang, T., Zhang, X., ... & Han, W. *Nano Energy*, 2024, **131**, 110285.
- Wang, L., Ning, H., Chen, S., Huang, Y., Chen, S., Wang, L., ... & Peng, J. *Applied Materials Today*, 2024, **41**, 102474.
- Liu, L., Zhang, Y., Tan, L., Deng, Y., Zheng, X., Tang, K., & Pei, Y. *Chemical Engineering Journal*, 2024, **499**, 155975.
- Li, Q., Zhang, Z., Xu, L., Wang, X., & Li, Z. *Sensors and Actuators A: Physical*, 2024, **378**, 115849
- Wang, J., Zhong, Y., Dai, S., Zhu, H., Wu, L., Gu, F., ... & Ding, J. *ACS Applied Nano Materials*, 2022, **5**(9), 13227-13235.
- Cheng, M., Yuan, Y., Li, Q., Chen, C., Chen, J., Tian, K., ... & Deng, H. *Journal of Materials Science & Technology*, 2025, **217**, 60-69.
- Amoli, V., Kim, J. S., Jee, E., Chung, Y. S., Kim, S. Y., Koo, J., ... & Kim, D. H. *Nature communications*, 2019, **10**(1), 4019.
- Kim, J. S., Choi, H., Hwang, H. J., Choi, D., & Kim, D. H. *Macromolecular Bioscience*, 2020, **20**(11), 2000147.
- Huang, H., Ran, X., Wan, S., Wang, Y., & Bi, H. *Nanoscale*, 2024, **16**(38), 17926-17933.
- Liu, C., Uddin, M. H., & Zhang, K. *Sensors and Actuators A: Physical*, 2024, **374**, 115519
- Zhou, Y., Zhao, L., Jia, Q., Wang, T., Sun, P., Liu, F., ... & Lu, G. *ACS Applied Materials & Interfaces*, 2022, **14**(49), 55109-55118.
- Bai, N., Wang, L., Xue, Y., Wang, Y., Hou, X., Li, G., ... & Guo, C. F. *Acs Nano*, 2022, **16**(3), 4338-4347.
- Lu, P., Wang, L., Zhu, P., Huang, J., Wang, Y., Bai, N., ... & Guo, C. F. *Science Bulletin*, 2021, **66**(11), 1091-1100
- Zhong, M., Zhang, L., Liu, X., Zhou, Y., Zhang, M., Wang, Y., ... & Wei, D. *Chemical Engineering Journal*, 2021, **412**, 128649
- Luo, J., Zhang, L., Wu, T., Song, H., & Tang, C. *Extreme Mechanics Letters*, 2021, **48**, 101279
- Zhen, L., Cui, M., Bai, X., Jiang, J., Ma, X., Wang, M., ... & Yang, B. *Nano Energy*, 2024, **131**, 110188.
- Chen, Y., Qin, C., Sun, Q., & Wang, M. *Sensors and Actuators A: Physical*, 2024, **379**, 115970. DOI: 10.1039/D5MH01784J
- Zhang, Y., Liu, C., Jia, B., Ma, D., Tian, X., Cui, Y., & Deng, Y. *npj Flexible Electronics*, 2024, **8**(1), 23.
- Sui, X., Mu, Q., Li, J., Zhao, B., Gu, H., Yu, H., ... & Hu, D. *Biosensors*, 2024, **14**(10), 508.
- Zhao, S., Chen, C., Wang, Z., Pan, C., & Yang, C. *InfoMat*, 2024, e12552.
- Xu, J., Li, H., Yin, Y., Li, X., Cao, J., Feng, H., ... & Zhu, G. *Flexible Electronics*, 2024, **6**(1), 62.
- Wan, C., Xiao, K., Angelin, A., Antonietti, M., & Chen, X. . *Advanced Intelligent Systems*, 2019, **1**(7), 1900073
- Mirza, S., Dobashi, Y., Glitz, E., Farajollahi, M., Mirabbasi, S., Naficy, S., ... & Madden, J. D, *Electroactive Polymer Actuators and Devices (EAPAD)*, 2015, 9430, 505-513
- Dobashi, Y., Yao, D., Petel, Y., Nguyen, T. N., Sarwar, M. S., Thabet, Y., ... & Madden, J. D, *Science*, 2022, **376**(6592), 502-507
- Xu, J., Li, Q., & Ho, D.. *Materials Horizons*, 2024, **11**(22), 5709-5721
- Dobashi, Y., Allegretto, G., Sarwar, M. S., Cretu, E., & Madden, J. D, *MRS Advances*, 2016, **1**(1), 63-68.
- Dai, J., Xue, Y., Chen, X., Cao, Z., Wang, L., Zhang, J., ... & Xiao, K. *Device*, 2024, **2**(7).
- Ma, B., Huang, K., Chen, G., Tian, Y., Jiang, N., Zhao, C., & Liu, *Soft Sci*, 2024, **4**:8
- Burattini, M., Lippens, R., Baleine, N., Gerard, M., Van Meerssche, J., Geeroms, C., ... & Thorrez, L. *Macromolecular Bioscience*, 2023, **23**(7), 2300019.
- Odent, J., Baleine, N., Biard, V., Dobashi, Y., Vancaeyzeele, C., Nguyen, G. T., ... & Raquez, J. M. *Advanced Functional Materials*, 2023, **33**(3), 2210485.
- Li, F., Cai, X., Liu, G., Xu, H., & Chen, W. *Advanced Functional Materials*, 2023, **33**(32), 2300701
- Zhu, W., Wu, B., Lei, Z., & Wu, P. *Advanced Materials*, 2024, **36**(18), 2313127.
- Ho, D. *ChemElectroChem*, 2024, **11**(3), e202300268.
- Chen, K., & Ho, D. *Aggregate*, 2024, **5**(1), e425.
- De Gennes, P. G., Okumura, K., Shahinpoor, M., & Kim, K. J, *Europhysics Letters*, 2000, **50**(4), 513.
- Song, Z., Cao, X., & Huang, H, *Physical Review E*, 2018, **97**(1), 012411.
- Song, Z., Cao, X., & Huang, H, *Physical Review E*, 2018, **98**(3), 032404.
- Wang, S., Yang, T., Zhang, D., Hua, Q., & Zhao, Y, *Advanced Materials*, 2024, **36**(36), 2405391.
- M. Kilic, M. Bazant, A. Ajdari, *Phys. Rev. E*, 2007, **75**, 021503
- Kim, Y. R., Lim, G., Cho, H., Kim, J., Kim, J., Yeom, J., ... & Ko, H, *Nano Energy*, 2024, **127**, 109749
- Zhao, J., Han, S., Yang, Y., Fu, R., Ming, Y., Lu, C., ... & Chen, W. *ACS nano*, 2017, **11**(9), 8590-8599
- Liu, Y., Hu, Y., Zhao, J., Wu, G., Tao, X., & Chen, W, *Small*, 2016, **12**(36), 5074-5080
- Lu, C., Yu, X., Chen, Y., Chen, X., & Zhang, X. *Chemical Engineering Journal*, 2023, **463**, 142523
- Lee, J. I., Choi, H., Kong, S. H., Park, S., Park, D., Kim, J. S., ... & Kang, M. S. *Advanced Materials*, 2021, **33**(29), 2100321.
- Li, L., Pan, J., Chang, L., Liu, Z., Wu, G., & Hu, Y. *Chemical Engineering Journal*, 2024, **482**, 148988
- Lu, Xi., Chen, Y., Zhang, Y., Cheng, J., Teng, K., Chen, Y., ... & An, Q. *Advanced Materials*, 2024, **36**(2), 2307875
- Li, L., Shao, Y., Jia, L., Guo, Z. H., Li, Z., Wang, Z. L., & Pu, X.. *Nano Energy*, 2025, **133**, 110477
- Adjaoud, A., Nguyen, G. T., Chikh, L., Peralta, S., Trouillet-Fonti, L., Uguen, N., ... & Plesse, C. *Smart Materials and Structures*, 2021, **30**(10), 105027.



REVIEW

Materials Horizons

- 63 Ming, Y., Yang, Y., Fu, R. P., Lu, C., Zhao, L., Hu, Y. M., ... & Chen, W. *Advanced Materials Technologies*, 2018, **3**(12), 1800257.
- 64 Lu, C., Chen, X., & Zhang, X. *ACS sensors*, 2023, **8**(4), 1624-1629
- 65 Lu, C., & Zhang, X. *Carbon*, 2024, **222**, 118956
- 66 Shevtsov, V.Y., Guerrero J., Nosov, D. R., Glinsek, S., Plesse, C., Odent, J., Raquez, J.-M., Shaplov, A.S. *ACS Sensors*, 2025, submitted.
- 67 Braz Ribeiro, F., Ni, B., Nguyen, G. T., Cattani, E., Shaplov, A. S., Vidal, F., & Plesse, C. *Advanced Materials Interfaces*, 2023, **10**(10), 2202381
- 68 Shaplov, A. S., Marcilla, R., & Mecerreyes, D. *Electrochimica Acta*, 2015, **175**, 18-34.
- 69 Shan, C., Wang, Y., Liang, M., Lu, K., Xiong, C., Hu, W., & Liu, B. *Energy Storage Materials*, 2023, **63**, 102955.
- 70 Zhu, Z., Chang, L., Horiuchi, T., Takagi, K., Aabloo, A., & Asaka, K. *Journal of Applied Physics*, 2016, **119**(12).
- 71 Gray-Weale, A. *Australian journal of chemistry*, 2009, **62**(4), 288-297
- 72 Hu, Y., & Suo, Z. *Acta Mechanica Sinica*, 2012, **25**(5), 441-458.
- 73 Wang, Q. M., Mohan, A. C., Oyen, M. L., & Zhao, X. H. *Acta Mechanica Sinica*, 2014, **30**, 20-27
- 74 Grenier, J., Duval, H., Barou, F., Lv, P., David, B., & Letourneur, D. *Acta Biomaterialia*, 2019, **94**, 195-203.
- 75 Matsushita, Y. *Encyclopedia of Polymeric Nanomaterials*, 2014, 1-6.
- 76 Wang, H., Xia, Y., Zhang, Z., & Xie, Z. *Journal of Materials Chemistry B*, 2023, **11**(37), 8883-8896.
- 77 Liu, G., Deng, Y., Ni, B., Nguyen, G. T., Vancaeyzeele, C., Brûlet, A., ... & Li, M. H. *Small*, 2024, **20**(12), 2307565.
- 78 Hu, F., Xue, Y., Xu, J., & Lu, B. *Frontiers in Robotics and AI*, 2019, **6**, 114.
- 79 Ates, H. C., Nguyen, P. Q., Gonzalez-Macia, L., Morales-Narváez, E., Güder, F., Collins, J. J., & Dincer, C. *Nature Reviews Materials*, 2022, **7**(11), 887-907.
- 80 Vaghasiya, J. V., Mayorga-Martinez, C. C., & Pumera, M. *npj Flexible Electronics*, 2023, **7**(1), 26.
- 81 Yoon, H. J., Lee, D. M., Kim, Y. J., Jeon, S., Jung, J. H., Kwak, S. S., ... & Kim, S. W. *Advanced Functional Materials*, 2021, **31**(23), 2100649
- 82 Denison, T., & Morrell, M. J. *Neurology*, 2022, **98**(2), 65-72.
- 83 Gupta, A., Vardalakis, N., & Wagner, F. B. *Communications biology*, 2023, **6**(1), 14.
- 84 Sezer, N., & Koç, M. *Nano energy*, 2021, **80**, 105567
- 85 Lei, Z., Xu, W., & Zhang, G. *Smart medicine*, 2023, **2**(1), e20220026.
- 86 Papani, R., Li, Y., & Wang, S. *Wiley Interdisciplinary Reviews: Nanomedicine and Nanobiotechnology*, 2024, **16**(3), e1961. Self-healing
- 87 Shen, Z., Ma, J., Cai, Y., Li, S., Ruan, D., Dai, S., ... & Jia, Z. *Cell Reports Physical Science*, 2023, **4**(12).
- 88 Wen, J., Tang, J., Ning, H., Hu, N., Zhu, Y., Gong, Y., ... & Huang, T. *Advanced Functional Materials*, 2021, **31**(21), 2011176.
- 89 Hansen, B. B., Spittle, S., Chen, B., Poe, D., Zhang, Y., Klein, J. M., ... & Sangoro, J. R. *Chemical reviews*, 2020, **121**(3), 1232-1285.
- 90 Khatib, M., Zohar, O., & Haick, H. *Advanced Materials*, 2021, **33**(11), 2004190.
- 91 Hu, J., Yao, X., Li, T., Li, X., Wei, W., & Liu, J. *ACS Applied Polymer Materials*, 2023, **5**(11), 9650-9658.
- 92 Liu, F. X., Jing, X., Yang, J., Mi, H. Y., Feng, F. Y., & Liu, Y. J. *Nano Today*, 2025, **61**, 102601.
- 93 Zhang, Z., Qian, L., Cheng, J., Ma, C., & Zhang, G. *Advanced Functional Materials*, 2024, **34**(37), 2402115.
- 94 Sun, B., Liu, K., Wu, B., Sun, S., & Wu, P. *Advanced Materials*, 2024, **36**(44), 2408826. Low hysteresis
- 95 Ezeokafor, I., Upadhya, A., & Shetty, S. *Frontiers in Neuroscience*, 2021, **15**, 671767. DOI: 10.1039/D5MH01784J

